UNIVERSITY OF BIRMINGHAM
University of Birmingham Research at Birmingham

Inflammation-induced formation of fat-associated lymphoid clusters

Bénézech, Cécile; Luu, Nguyet-Thin; Walker, Jennifer A; Kruglov, Andrei A; Loo, Yunhua; Nakamura, Kyoko; Zhang, Yang; Nayar, Saba; Jones, Lucy H; Flores-Langarica, Adriana; McIntosh, Alistair; Marshall, Jennifer; Barone, Francesca; Besra, Gurdyal; Miles, Katherine; Allen, Judith E; Gray, Mohini; Kollias, George; Cunningham, Adam F; Withers, David R

DOI:
10.1038/ni.3215

License:
Other (please specify with Rights Statement)

Document Version
Peer reviewed version

Citation for published version (Harvard):
Bénézech, C, Luu, N-T, Walker, JA, Kruglov, AA, Loo, Y, Nakamura, K, Zhang, Y, Nayar, S, Jones, LH, Flores-Langarica, A, McIntosh, A, Marshall, J, Barone, F, Besra, G, Miles, K, Allen, JE, Gray, M, Kollias, G, Cunningham, AF, Withers, DR, Toellner, KM, Jones, ND, Veldhoen, M, Nedospasov, SA, McKenzie, ANJ & Caamaño, JH 2015, 'Inflammation-induced formation of fat-associated lymphoid clusters', *Nature Immunology*, vol. 16, no. 8, pp. 819-828. https://doi.org/10.1038/ni.3215

Link to publication on Research at Birmingham portal

Publisher Rights Statement:
Final Version of Record available online at: http://dx.doi.10.1038/ni.3215

Eligibility for repository checked August 2015

General rights
Unless a licence is specified above, all rights (including copyright and moral rights) in this document are retained by the authors and/or the copyright holders. The express permission of the copyright holder must be obtained for any use of this material other than for purposes permitted by law.

•Users may freely distribute the URL that is used to identify this publication.
•Users may download and/or print one copy of the publication from the University of Birmingham research portal for the purpose of private study or non-commercial research.
•User may use extracts from the document in line with the concept of 'fair dealing' under the Copyright, Designs and Patents Act 1988 (?)
•Users may not further distribute the material nor use it for the purposes of commercial gain.

Where a licence is displayed above, please note the terms and conditions of the licence govern your use of this document.

When citing, please reference the published version.

Take down policy
While the University of Birmingham exercises care and attention in making items available there are rare occasions when an item has been uploaded in error or has been deemed to be commercially or otherwise sensitive.

If you believe that this is the case for this document, please contact UBIRA@lists.bham.ac.uk providing details and we will remove access to the work immediately and investigate.

Download date: 03. May. 2024

“Inflammation-induced formation of fat-associated lymphoid clusters”

Cécile Bénézech[1,11], Nguyet-Thin Luu[1,12], Jennifer A. Walker[2,12], Andrei A. Kruglov[3,4,5], Yunhua Loo[6], Kyoko Nakamura[1], Yang Zhang[1], Saba Nayar[1], Lucy H. Jones[7,11], Adriana Flores-Langarica[1], Alistair McIntosh[1], Jennifer Marshall[1], Francesca Barone[1], Gurdyal Besra[8], Katherine Miles[9], Judith E. Allen[7], Mohini Gray[9], George Kollias[10], Adam F. Cunningham[1], David R. Withers[1], Kai Michael Toellner[1], Nick D. Jones[1], Marc Veldhoen[6], Sergei A. Nedospasov[3,4,5], Andrew N.J. McKenzie[2] & Jorge H. Caamaño[1]

[1]School of Immunity and Infection, IBR-MRC Centre for Immune Regulation, College of Medical and Dental Sciences, University of Birmingham, Birmingham, B15 2TT, UK, [2]MRC Laboratory of Molecular Biology, Cambridge, UK, [3]German Rheumatism Research Center, Berlin, Germany, [4]Engelhardt Institute of Molecular Biology and [5]Lomonosov Moscow State University, Moscow, Russia, [6]Lymphocyte Signalling and Development Programme, The Babraham Institute, Cambridge, UK, [7]Institute of Immunology and Infection Research, University of Edinburgh, Edinburgh, [8]College of Life and Environmental Sciences, University of Birmingham, Birmingham, UK, [9]Centre for Inflammation Research, University of Edinburgh, Edinburgh, UK, [10]Fleming Institute, Athens, Greece.

Correspondence should be addressed to C.B. (cbenezec@ed.ac.uk) or J.H.C. (j.caamano@bham.ac.uk).

[11]Present address: BHF/UoE Centre for Cardiovascular Sciences, University of Edinburgh, Edinburgh, UK
[12]These authors contributed equally to this work

Running Title: iNKT cells and TNF are required for FALC formation

ABSTRACT

Fat-associated lymphoid clusters (FALCs) are a recently discovered type of lymphoid tissue associated with visceral fat. Here we show that distribution of FALCs was heterogeneous with the pericardium containing large numbers of these clusters. FALCs contributed to the retention of B-1 B cells in the peritoneal cavity through high expression of the chemokine CXCL13 and supported B cell proliferation and germinal center differentiation during peritoneal immune challenges. FALC formation was induced by inflammation, which triggered recruitment of myeloid cells that express tumor necrosis factor (TNF) necessary for TNF receptor-signaling in stromal cells. CD1d-restricted Natural killer T (NKT) cells were likewise required for inducible formation of FALCs. Thus, FALCs support and coordinate innate B and T cell activation during serosal immune responses.

INTRODUCTION

The peritoneal and pleural cavities support rapid immune responses when the integrity of the intestine or the lungs is compromised or lost. They contain innate-like B cell populations producing natural antibodies vital for the early control of infections, protecting against auto-immunity and contributing to adaptive immunity[1-7]. These B-1 cells recirculate between the peritoneal space and the omentum[8], a sheet of intra-abdominal adipose tissue containing lymphoid structures called "milky spots"[9-12]. Upon peritoneal inflammation the number and size of milky spots increases and the recruitment of lymphocytes and macrophages phagocytosing particles and pathogens is substantially augmented[9, 11, 12]. The omentum also acts as a secondary lymphoid structure that promotes immunity to peritoneal antigens[10, 12].

The existence of B cell-rich clusters in adipose tissue (AT) has recently been extended to the rest of the visceral fat in the peritoneal and pleural cavity[13, 14]. Moro and collaborators named them Fat Associated Lymphoid Clusters (FALCs)[14]. Their presence was associated with the presence of Group 2 innate lymphoid cells (ILC2)[14-17] in visceral AT, yet no direct evidence has shown that ILC2s induce formation of FALCs[14]. The exact composition of these clusters, their relative distribution in AT as well as their function and the mechanisms regulating their formation remain unknown.

Here we show that the distribution of lymphoid structures in AT was very heterogeneous, with the omentum, the pericardium and mediastinum being the tissues that contained the largest number of FALCs. We report that the development of FALCs was regulated by unique cellular and molecular mechanisms that, in contrast to other secondary lymphoid tissues, did not involve lymphoid tissue inducer (LTi) cells, ILC3s or the lymphotoxin beta receptor (LTβR) pathway[18-20]. Their postnatal formation was partly dependent on tumor necrosis factor receptor (TNFR) signaling and the presence of the commensal flora. FALC stromal cells expressed high amounts of the chemokine CXCL13 that was crucial for the recruitment and retention of B cells in the clusters. Inflammation-induced formation of FALCs required TNF expression by myeloid cells and TNFR-signaling in stromal cells. Peritoneal immunization with T-independent and T-dependent antigens induced B cell differentiation into plasma cells and germinal center (GC)-like B cells in FALCs indicating an important function of these clusters during immune responses. Finally, we show that CD1d-restricted natural killer T (NKT) cells, a subset of T cells enriched in ATs, and interleukin 13 (IL-13) played a key role in inflammation-induced FALC formation.

RESULTS

Visualization and characterization of FALCs

Whole-mount immunofluorescence staining of the main visceral AT allowed, with a fluorescence stereomicroscope, the visualization (**Fig. 1a**) and enumeration of the $CD45^+$ cell clusters present in the omental, gonadal, mesenteric, mediastinal and pericardial fat. In the peritoneal cavity, the omentum was the fat depot with the highest density of lymphoid clusters (8000 clusters/g) with a mean of 80 milky spots per omentum. The mesenteric fat depot contained a median of 120 clusters/g with a mean of 16 clusters per mesentery while gonadal AT had 8 clusters/g with a mean of 1–2 clusters per depot (**Fig. 1b)**. In the pleural cavity, the pericardium had the highest density of lymphoid clusters (5400 clusters/g) with a mean of 40 clusters per tissue. The mediastinum with a density of 2100 clusters/g and a mean of 9 clusters per mediastinum, accounted for the rest of the FALCs in the pleural cavity (**Fig. 1b**). This analysis revealed the high heterogeneity in the lymphoid cluster content of ATs.

The cellular composition of the clusters was characterized using whole mount immunofluorescence staining of mouse mesenteries with anti CD4, CD45, IgM and CD11b Abs followed by confocal microscopy analysis. In resting conditions FALCs were mostly composed of IgM^+ B cells, with low numbers of $CD4^+$ T cells and $CD11b^+$ myeloid cells (**Fig. 1c** and **Supplementary Fig.1**). Clusters of different sizes and degrees of B-T cell segregation could be observed in individual mice (**Supplementary Fig.1**). A fraction of B cells expressed CD11b and abundant surface IgM, indicating that these were likely B-1 B cells. We did not detect any differences in the hematopoietic composition of FALCs from the mesenteries, mediastinum or pericardium that resembled the milky spots of the omentum (data not shown). FALCs appeared to be highly vascularized, as shown by the presence of $CD31^+$ blood vessels. However, no clear connection with Lyve-1^+ lymphatic vasculature could be detected. Only scattered Lyve-1^+ macrophages were seen in close proximity of FALCs (**Fig. 1d**).

The mesenteric ATs, where FALCs were easier to identify and enumerate, were used in the rest of the study. FALC formation was initiated after birth, with the first clusters identified in the mesenteries of two- to three-week old animals and their number increasing to reach a plateau at around 18 weeks of age (**Fig. 1e**). These results showed that FALCs are present in different visceral ATs in variable numbers and contained mainly B cells, with low numbers of T and myeloid cells.

CXCL13 is highly expressed by stromal cells in FALCs

To understand how B and T cells were recruited to FALCs, we assessed the expression of genes encoding the homeostatic chemokines *Cxcl13*, *Ccl21* and *Ccl19* and the cytokine *Il7* by qPCR analysis in isolated clusters. *Cxcl13* expression was particularly high in FALCs as compared to the associated AT (>100 fold) or lymph nodes (LN) (10 fold). In contrast, *Ccl21*, *Ccl19* and *Il7* transcripts were not enriched in FALCs compared to the other tissues analyzed (**Fig. 2a**). In agreement with these findings, the number and composition of FALCs in CCL21- and CCL19-deficient mice (*plt/plt)* and *Ccr7*$^{-/-}$ mice presented no differences with their wild-type counterparts (**Fig. 2b)**. *Tnf* and *Ltb* transcripts were both highly expressed in FALCs, which might reflect the high content of B cells in these clusters.

Immuno-fluorescence staining revealed the presence of CD45^{-}CXCL13^{+} stromal cells with an elongated morphology (**Fig. 2d**) that resembled follicular dendritic cells (FDCs). LTβR and/or TNFR signaling is involved in inducing *Cxcl13* expression in spleen and LN FDCs[21-23]. However, CXCL13^{+} cells were present in FALCs of *Ltbr*$^{-/-}$, TNFR1-TNFR2 double-deficient (*Tnfrsf1a*$^{-/-}$*Tnfrsf1b*$^{-/-}$) and *Rag2*$^{-/-}$ mice, demonstrating that CXCL13 expression by FALC stromal cells was independent of signals induced by these receptors and the presence of lymphocytes (**Fig. 2d**)[24, 25].

To test whether CXCL13 expression was required for the recruitment of B cells in FALCs, we analyzed the *Cxcr5*$^{-/-}$ mice, deficient for the CXCL13 receptor. A normal number of FALCs formed in the mesenteries of these mice, but the number of B cells present in the clusters was markedly reduced. Thus, CXCL13 was not important for FALC formation but was essential for the recruitment of B cells (**Fig. 2b,c**). These data are consistent with previous reports showing that mesenteric and omentum tissues are important sources of CXCL13 required for the retention of peritoneal B cells. Overall, we demonstrate that the presence of CXCL13 in the mesenteries is due to its specific expression by FALC stromal cells and not the surrounding VAT.

FALCs support B cell proliferation and differentiation

B-1 cells are important for immune responses against T-independent (TI) antigens[2, 5, 26-31]. To assess B cell responses in FALCs, we used the TI antigen 4-hydroxy-3-nitrophenylacetyl (NP)-Ficoll to immunize QM/QM (*Igh*$^{NP/NP}$*Igk*$^{-/-}$) mice, which have a

quasi-monoclonal primary B cell repertoire specific for NP[32]. Flow-cytometric analysis of the proliferation marker Ki67 revealed that both B-1 and B-2 cells were proliferating in the mesenteries 24 h post intraperitoneal immunization. The percentage of $Ki67^+$ proliferating B-1 cells was three times higher in the mesenteries than in the peritoneal cavity lavage or the spleen, reaching 70% for $CD5^+$ B-1a, 50% for $CD5^-$ B-1b and 40% for $CD5^+CD11b^-$ B-1c cells. Up to 40% of B2 cells also proliferated in response to NP-Ficoll (**Supplementary Fig. 2a,b**). Whole mount staining of the mesenteries 24 h after immunization showed a marked enlargement of FALCs and an increased frequency of IgM^+ cells (**Supplementary Fig. 2c**).

To confirm that FALC B cells secreted IgM, we assessed the number of antibody-forming cells (AFCs) in QM × C57BL/6 (B6) ($Igh^{NP/wt}Igk^{-/wt}$) mice[33], which contain 5% of NP-specific B cells, four days after NP-Ficoll IP immunization. ELISPOT analysis confirmed an expansion of NP-specific B cells expressing IgM in the immunized animals (**Fig. 3a** top) as well as a significant increase in the number of IgG^+ AFC in FALCs and spleen (**Fig. 3a** bottom and **Fig. 3b**). Further evidence of Ig switching in FALCs was obtained by NP-Ficoll immunization of C_γ1-CrexQMmTmG mice ($Igh^{NP/C_\gamma1Cre}$ $Igk^{-/-}$ $mTmG^{+/wt}$). These mice carry one copy of the Cre recombinase gene in the constant region of the Cγ1 *Igh* gene, one copy of the NP-specific *Igh* from QM mice and the membrane Tomato membrane Green (mTmG) reporter. NP immunization induced B cell activation and Ig class switching with the concomitant expression of Cre recombinase that resulted in the membrane reporter switch from IgM (red) to IgG (green). Whole mount immuno-fluorescence analysis revealed that NP-Ficoll immunisation induced the appearance of clusters of class-switched green B cells in the mesenteries (**Fig. 3b**). The early and preferential proliferation of B-1 cells in FALCs, and the presence of IgM- and IgG-producing cells demonstrated that these clusters contribute to peritoneal cavity B-1 cells immune responses to type II antigens.

The role of FALCs in T-dependent immune responses was tested by adoptive transfer of peritoneal lavage cells from QM/QM $EYFP^{+/-}$ mice into C57BL/6J recipients that were immunized subsequently with alum precipitated–NP-ovalbumin (OVA) by intraperitoneal injection. Flow cytometric analysis of cells isolated eight days after immunization showed a statistically significant increase in the frequency and number of Ag-specific B cells and $CD38^-GL7^+$ GC-like B cells in FALCs, spleen and mesenteric (m)LNs (**Fig. 3c,d** and data not shown). An endogenous immune response was elicited by intraperitoneal immunization of C57BL/6J mice with alum precipitated-phycoerythrin (PE). In agreement with the results above, flow-cytometric analysis of FALCs, spleen and mLN

showed a 20-fold increase in the proportion and number of PE-specific B cells and GC-like B cells (**Fig. 3e,f** and data not shown). Taken together, these results indicate that FALCs function as lymphoid tissues by supporting early activation of B cells during inflammation and differentiation towards plasma cells and germinal center cells during adaptive immune responses in the peritoneal cavity.

Cells and signals required for FALC development

The development of LNs and Peyer's patches is dependent on the activity of LTi cells and engagement of the LTβR[18-20]. To determine whether the formation of FALCs followed the same cues, we assessed their presence in the *Ltbr*$^{-/-}$, *Lta*$^{-/-}$ and *Rorc*$^{-/-}$ mouse strains in which LN development is fully impaired[34-36]. The number and composition of FALCs in these strains was identical to wild-type mice, indicating that the development of FALCs was independent of LTi or ILC3 cells and LTβR engagement (**Fig. 4a,b**). To determine whether any other lymphoid cell type was involved in FALC formation, we analyzed *Rag2*$^{-/-}$ mice, lacking lymphocytes, and *Rag2*$^{-/-}$*Il2rg*$^{-/-}$ mice that are deficient in lymphocytes and ILCs. FALCs were present in normal numbers in *Rag2*$^{-/-}$ mice, however they were absent in *Rag2*$^{-/-}$*Il2rg*$^{-/-}$ mice, revealing a potential requirement for ILCs and/or NK cells to initiate cluster formation. *Il15*$^{-/-}$ mice have similar FALC numbers to their wild-type counterparts, ruling out a role for NK cells in the formation of these clusters (data not shown). Flow cytometric analysis of AT in wild-type and *Rag2*$^{-/-}$ mice demonstrated the presence of Lin^{-} c-Kit^{+}Sca-1^{+}IL-7Rα^{+} type 2 ILCs (**Supplementary Fig. 3a**). Over 80% of the Lin^{-} CD90^{+}Sca-1^{+}NK1.1^{-} cells present in FALCs of *Rag2*$^{-/-}$ mice were ILC2 cells (**Supplementary Fig. 3b**). Immunofluorescence staining of mesenteries of *Rag2*$^{-/-}$ mice also identified clusters of CD90^{+}CD11b^{-} cells in FALCs corresponding to ILCs (**Supplementary Fig. 3c**).

As the LTα-LTβR pathway was not required for the formation of FALCs, we examined the role of TNF, another key regulator of lymphoid tissue organization[22, 23, 37]. We observed half the number of FALCs as well as reduced cluster size in *Tnfrsf1a*$^{-/-}$ *Tnfrsf1b*$^{-/-}$ mice as compared to wild-type mice (**Fig. 4a,b**). Conversely, in the *Tnf*$^{+/\Delta ARE}$ mice, which carry a deletion that results in the accumulation of *Tnf* mRNA and TNF protein, we observed an eight-fold increase in FALC numbers and in the size of the clusters as compared to wild-type littermates (**Fig. 4a,b**). Thus, we conclude that TNF signaling promoted the formation of FALCs.

Colonization by the commensal flora is involved in the postnatal development and maturation of the gut-associated lymphoid tissues (GALT)[38-41]. Germ-free mice showed a two-fold reduction in the number of FALCs, indicating that the commensal flora partly contributed to their formation (**Fig. 4a,b**). Overall, these analyses revealed that the formation of FALCs is dependent on an innate lymphoid cell type different from LTi cells and other RORγt$^+$ ILC3 cells and partly dependent on TNF signaling and colonization by the commensal flora.

Peritoneal inflammation led to rapid formation of FALCs

Since the formation of FALCs was increased in *Tnf*$^{+/\Delta ARE}$ mice, we tested the effect of acute sterile peritonitis on cluster formation. Peritoneal inflammation driven by zymosan led to a marked increase in the size and number of FALCs at day 3, with the clusters becoming visible without counterstaining under the dissecting microscope (**Fig. 4c**) and their numbers doubling (**Fig. 4d**). Immuno-fluorescence staining showed that this was associated with the recruitment of CD11b$^+$ myeloid cells (**Fig. 4e**) that were mostly Gr1$^{lo/-}$ Ly6C$^{lo/-}$F4/80$^+$ macrophages (**Supplementary Fig. 4**). Thus, peritoneal inflammation leads to a general expansion of FALCs.

TNF signals induced FALC formation

To test the hypothesis that TNF contributed to FALC formation, *Tnfrsf1a*$^{-/-}$*Tnfrsf1b*$^{-/-}$ mice were immunized with zymosan. Even though existing FALCs increased in size and recruited CD11b$^+$ myeloid cells, zymosan failed to induce *de novo* formation of clusters at day 3 post-injection in this knockout strain. (**Fig. 5a**). We then asked whether TNFR-signaling was required on stromal cells to induce formation of FALCs following zymosan injection. Wild-type and *Tnfrsf1a*$^{-/-}$*Tnfrsf1b*$^{-/-}$ recipient mice were lethally irradiated, reconstituted with wild-type bone marrow donor cells and received an intraperitoneal injection of zymosan. Reconstitution of *Tnfrsf1a*$^{-/-}$*Tnfrsf1b*$^{-/-}$ recipient mice with wild-type donor bone marrow did not rescue FALC formation upon inflammation at day 3 post-injection as it did in the control wild-type recipient mice bone marrow chimeras (**Fig. 5b**). Thus, our data indicate that radiation-resistant stromal cells respond to TNF and induce FALC formation.

To determine the cellular origin of TNF, we used mouse strains with specific deletion of *Tnf* in either CD4$^+$ T cells (T-TNF, *Cd4*-Cre), B cells (B-TNF, *Cd19*-Cre) or

macrophages/neutrophils (M-TNF, *Lysm*-Cre). Specific ablation of *Tnf* in T and B cells did not impair the induction of cluster formation upon inflammation as seen by the 3- and 2-fold increase in cluster numbers observed in T-TNF and B-TNF mice, respectively (**Fig. 5c**). In contrast, loss of *Tnf* expression by neutrophils and macrophages in M-TNF mice resulted in the absence of new FALC formation following zymosan injection, even though $CD11b^+$ myeloid cells were recruited to the clusters (**Fig. 5c**). Intracellular flow-cytometric analysis confirmed that TNF^+ cells were of myeloid origin (data not shown) with 40% of $F4/80^+$ macrophages and $Ly6C^{hi}F4/80^-$ monocytes displaying intra-cellular TNF expression in the mesenteries after zymosan injection (**Fig. 5d**). Once correlated to their cell number, macrophages represented 60% of all TNF^+ myeloid cells in the mesenteries (**Fig. 5d**). Taken together, these results demonstrate the importance of macrophages as a key source of TNF and TNFR signaling in stromal cells for *de novo* formation of FALCs upon inflammation.

FALC formation upon inflammation required iNKT cells

Given the prevalence of B cells in FALCs, we evaluated their role in inducible formation of these clusters. To do so, we analyzed the effect of intraperitoneal injection of zymosan in *Rag2*$^{-/-}$ mice, lacking T and B cells, and in B cell-deficient *Ighm*$^{-/-}$ mice. B cells were not involved in FALC formation as shown by the three-fold increase in their number (**Fig. 6a**) and the recruitment of $CD11b^+$ myeloid cells (**Fig. 6b**). However, peritoneal inflammation failed to induce cluster formation in *Rag2*$^{-/-}$ mice, indicating a requirement for T cells (**Fig. 6a**). This result was confirmed in Tg(CD3E)26Cpt mice, in which the development of T, NK and NKT cells is blocked. In both *Rag2*$^{-/-}$ and Tg(CD3E)26Cpt mice, inflammation induced a normal recruitment of myeloid cells in FALCs (**Fig. 6a,b**). $\gamma\delta$ T cells were not involved in FALC formation upon peritoneal inflammation as shown by a five-fold increase in the number of FALCs in *Tcrd*$^{-/-}$ mice following zymosan injection (**Fig. 6a,b**).

We next assessed the role of CD1d-restricted natural killer T (NKT) cells in inducible FALC formation. Injection of zymosan failed to induce cluster formation at day 3 post-injection in *Cd1d*$^{-/-}$ mice (**Fig. 6a,b**). This result indicated an important role for NKT cells in FALC formation.

Activation of iNKT cells induces FALCs formation

NKT cells recognize lipid-based antigen presented by CD1d. The best characterized NKT cell population is the CD1d-restricted invariant NKT cell (*i*NKT) population due to their TCRα chain usage (in mice encoded by the *Tcra* Vα14-Jα18 gene segments). *i*NKT cells recognize and strongly respond to the synthetic glycolipid α-galactosylceramide (α-GalCer) presented on CD1d[28]. Previous studies have described the presence of *i*NKT cells in AT and their role in regulation of metabolism[42-46]. Flow cytometric analysis using anti-CD3ε Abs and CD1d-PBS-57 tetramer confirmed that *i*NKT cells were particularly enriched in ATs, representing up to 6% of all lymphocytes, compared to the spleen or the mLNs that contained approximately 0.03% or 0.1% *i*NKT cells, respectively (**Fig. 7a**). To detect *i*NKT cells *in situ*, we transferred CD1d-PBS-57 tetramer-isolated CFSE-labeled *i*NKT cells into wild-type mice and showed that these cells were indeed recruited to FALCs (**Fig. 7b**).

We next tested the effect of *i*NKT cell activation on FALC formation by intraperitoneal injection of α-GalCer into wild-type mice. α-GalCer elicited a two-fold increase in the number of clusters as compared to control that received vehicle. This observation demonstrated that direct TCR activation of *i*NKT cells was sufficient to induce cluster formation (**Fig. 7c**). We then assessed whether TNFR pathways were also required for cluster formation following TCR activation of *i*NKT. FALC formation upon α-GalCer injection was abrogated in *Tnfrsf1a*$^{-/-}$*Tnfrsf1b*$^{-/-}$ mice, indicating the need for signaling through these receptors (**Fig. 7d**).

To test whether *i*NKT cells were sufficient to rescue inflammation-induced FALC formation in *Rag2*$^{-/-}$ mice, we transferred sorted splenic *i*NKT cells or CD3^{hi} cells by intraperitoneal injection in these mice, 24 h before immunization with zymosan. Only mice that received *i*NKT cells showed an increase in FALC numbers after zymosan injection (**Fig. 7e**).

We next tested the effect of the selective loss of *i*NKT cells on the formation of FALCs upon zymosan-induced inflammation. FALC numbers were increased two-fold in mice lacking the *Tcra* Jα18 gene segment following zymosan injection (**Fig. 7f**) indicating that *i*NKT cells were not absolutely required for formation of these clusters. Taken together, these results indicate that even though *i*NKT cells were sufficient to restore cluster formation in *Rag2*$^{-/-}$ mice, the function of *i*NKT cells and other non invariant CD1d restricted NKT cells appear to be overlapping during inflammation-induced FALC formation.

FALC formation upon inflammation required IL-4Rα

Upon activation, *i*NKT cells produce very rapidly large amounts of T_H1 or T_H2 cytokines (IFN-γ or IL-4, respectively), that link innate and adaptive immune responses and play important immunoregulatory functions[28]. To understand the involvement of T_H1 and T_H2 cytokines in inflammation-induced FALC formation, we tested the effect of zymosan-induced inflammation in mice deficient in either of these cytokines. FALC formation induced by the injection of zymosan was not impaired in *Ifng*$^{-/-}$ mice, indicating that IFN-γ was not required (**Supplementary Fig. 5**).

In contrast, zymosan injections failed to induce formation of new clusters at day 3 post-injection in *Il4ra*$^{-/-}$ mice, where signaling by IL-4 and IL-13 is impaired, while BALB/c wild-type mice responded with a two-fold increase in the number of FALCs (**Fig. 8a,b**). FALC numbers were two-times higher in the BALB/c mouse strain compared to the C57BL/6J strain, suggesting that the T_H2 bias shown in the former contributed to their higher number of FALCs.

To determine the respective contribution of IL-4 and IL-13, we studied FALC formation in the *Il4*$^{-/-}$ and *Il13*$^{-/-}$mouse strains. In both mutant strains zymosan injection led to the formation of new clusters, suggesting that these cytokines exerted redundant functions in the BALB/c background (**Fig. 8a,b**). However, IL-13 played a critical role in inflammation induced FALC formation in the C57BL/6J background as shown by the absence of new cluster formation in *Il13*$^{-/-}$ mice at day 3 post-injection (**Fig. 8c**). To test whether IL-13 produced by *i*NKT cells was sufficient to rescue the inducible FALC formation in *Il13*$^{-/-}$mice, we transferred sorted splenic *i*NKT cells into these mice, 24 h before immunization with zymosan. We found that IL-13-sufficient *i*NKT cells induced a slight increase in FALC numbers in *Il13*$^{-/-}$ mice but this did not reach statistical significance (**Fig. 8c**). These results indicate that *i*NKT production of IL-13 contributes to inflammation-induced FALC formation, but that additional sources of IL-13 may be required. We finally assessed the role of IL-4Rα signaling in the formation of FALCs driven by direct *i*NKT cell activation. α-GalCer injection failed to induce FALCs formation in *Il4ra*$^{-/-}$ mice (**Fig. 8d**). These findings indicate that formation of FALCs through direct activation of *i*NKT cells also required IL-4Rα signaling.

IL-4 partially rescued FALC formation in absence of TNF

Our results showed that TNFR and IL-4Rα signaling were necessary for inflammation-induced FALC formation. To test whether crosstalk between these receptors was necessary, we performed a serie of combinatorial and rescue experiments. Injection of TNF and IL-4-anti IL-4 complex (IL-4c) alone or in combination was not sufficient to induce cluster formation (**Supplementary Fig. 6a**), indicating that other factors were involved in this process. Intraperitoneal injection of TNF could not rescued zymosan-induced FALC formation in *Il4ra*$^{-/-}$ mice. In contrast, intraperitoneal injection of IL-4c in *Tnfrsf1a*$^{-/-}$ *Tnfrsf1b*$^{-/-}$ mice induced a small but significant increase in the number of zymosan-induced FALCs, indicating that IL-4 could partially rescue cluster formation in the absence of TNFR signaling and thus may act downstream of TNF (**Supplementary Fig. 6b**).

DISCUSSION

In this report we defined the requirements for the formation of a new type of lymphoid tissue called Fat Associated Lymphoid Clusters. In the peritoneal cavity, mesenteric FALCs and omental milky spots accounted for the quasi-totality of the lymphoid clusters associated with AT. In the pleural cavity, the pericardium and mediastinum showed a density of lymphoid clusters approaching the levels of the omentum. FALCs contained a high proportion of B1 cells with no apparent B and T cell segregation, comparable to what has been reported previously for the milky spots of the omentum[12]. FALCs expressed high levels of CXCL13 required for efficient recruitment of B cells, which upon immune challenge with T-dependent or -independent antigens actively proliferate, and undergo differentiation towards plasma cells or GC cells in these clusters. The function of FALCs and milky spots are probably overlapping in the peritoneal cavity, but FALCs contained in the mediastinal and the pericardial fat are likely to be the main sites for the organization of immune responses and for retention of B1 cells by CXCL13 in the pleural cavity.

FALC development in mice was constitutive and its initiation coincided with weaning. Establishment of a normal number of FALCs in adult mice was dependent on TNFR signaling and colonisation by commensal flora suggesting a role for Pattern Recognition Receptors. FALCs were totally absent in *Rag2*$^{-/-}$*Il2rg*$^{-/-}$ mice and immunofluorescence and flow-cytometric analysis in *Rag2*$^{-/-}$ mice indicated that cells present in the clusters in absence of T and B cells were ILCs. Importantly, FALC formation was independent of the presence of LTi cells and other ILC3 cells as well of LTαβ-LTβR-signaling which resembles the formation of nasal associated lymphoid tissues (NALT)[47].

Peritoneal inflammation induced a rapid neo-formation of a large number of FALCs reaching a two- to three-fold increase compared to resting conditions. This effect was dependent on TNF expression by myeloid cells and TNFR signaling on stromal cells. Coupling of inflammation and rapid FALC formation provide a platform to link innate and adaptive immune responses that support rapid B cell proliferation and natural antibody secretion in the body cavities following infection. Neo-formation of FALCs also necessitated the activation of *i*NKT cells and signaling through the IL4Rα. Interestingly, triggering of *i*NKT cells through TCR ligation was sufficient to induce formation of FALC that was also dependent on TNFR and IL-4Rα signaling. Therefore, induction of FALC formation seemed to require both an inflammatory signal, delivered by TNF, and a Th2/Resolution signal transduced by IL-4Rα. How FALC formation is timed with the iniation of the resolution of inflammation and whether FALCs play a role in the resolution phase remains to be investigated.

We and others have recently shown that ATs constitute an important reservoir of stem cells for the formation of lymphoid stroma in LNs during development[22, 48] and immune responses[49]. It is thus conceivable that FALC stromal cells originate from AT stem cells or peri-vascular cells, as has been recently shown for FDCs[22].

This work constitutes the first report of NKT cells having a lymphoid organogenic activity. Not only were NKT cells necessary for the formation of FALCs during inflammation, but also their sole activation was sufficient to induce neo-formation of clusters. A number of studies have recently highlighted the role of NKT cells in the regulation of AT metabolism in normal nutrient homeostasis and during obesity[42-46]. Whether the metabolic activity of NKT cells is linked to their capacity to induce FALC formation and alter the homeostasis of other hematopoietic cells present in ATs remains to be investigated.

ACKNOWLEDGMENTS

We are grateful to the personnel in BMSU for taking care of our animal colonies. We want to thank E. Jenkinson for continuous support. We are thankful to G. Anderson, P. Lane, and A. Rot for comments on the manuscript. We are also thankful to C. Buckley for facilitating animal procedures and to R. Bird for cell sorting. We are indebted to K. Pfeffer (Heinrich Heine Univ. Dusseldorf, Germany), G. Eberl (Institut Pasteur, France), D. Finke (Univ. of Basel, Switzerland), and A. Diefenbach (Univ. of Mainz, Germany) for providing mouse strains and reagents. CD1d-PBS57 loaded tetramers were kindly provided by the National Institutes of Health Tetramer Facility (Atlanta GA, USA).

This work was supported by the EU FP7 integrated project INFLACARE and a BBSRC grant (BB/K004900/1) to J. Caamaño. The work in A. McKenzie laboratory was supported by the American Asthma Foundation, UK-MRC and the Wellcome Trust (grant number 100963/Z/13/Z). M. Veldhoen laboratory was supported by the BBSRC institute synergy programme grant, and ERC grant (280307). Work in S. Nedospasov laboratory was supported by DFG (NE1466/2-1) and a grant from Russian Science Foundation (14-50-00060) and grant to A.A.K from RFBR (13-04-40268). G. Kollias laboratory was supported by ERC grant 340217 - MCs_inTEST. S. Nayar was the recipient of an MRC DTA PhD studentship. LHJ was funded by the UK-MRC (MRC/K01207X/1). YL was supported by a MB/PhD scholarship from the Agency of Science, Technology and Research (A*STAR). KMT, YZ and JM were supported by a grant through the Lifelong Health and Wellbeing cross council initiative (Topjabs G1001390).

AUTHOR CONTRIBUTIONS

C.B., N-T.L., J.A.W., A.A.K., Y.L., K.N., Y.Z., S.N, L.H.J. and J.H.C. designed and performed the research, collected and analyzed the data. A.F-L., A.M., J.M., F.B., G.B., K.M., J.E.A., M.G., G.K., A.F.C., D.R.W., K.M.T., N.D.J., M.V., S.A.N. and A.N.J.M. facilitated the research. C.B. and J.H.C. wrote the manuscript.

COMPETING FINANCIAL INTERESTS

The authors declare that there is no conflict of financial interest.

FIGURE LEGENDS

Figure 1. Distribution of FALCs in VAT.

(**a**) Whole mount immunofluorescence staining of the mesenteries allowing visualisation of $CD45^+$ FALCs (green). (**b**) Density of hematopoietic clusters (number of clusters/g adipose tissue) in the main fat deposits of the peritoneal (omental (n=8 mice), gonadal (n=7) and mesenteric (n=6) adipose tissues) and pleural cavities (mediastinal (n=13) and pericardial (n=8) adipose tissues) and in the subcutaneous fat (n=7). Data points and mean shown. Data pooled from two independent expts. (**c**) Whole mount immunofluorescence staining showing a mesenteric FALC with $CD11b^+$ myeloid cells (blue), $CD45^+$ hematopoietic cells (green), IgM^+ B cells (red), and $CD4^+$ T cells (white). Picture representative of clusters from multiple independent experiments. (**d**) Whole mount immunofluorescence staining showing a mesenteric FALC with $CD45^+$ hematopoietic cells (green), $CD31^+$ blood endothelial cells (red) and Lyve-1^+ cells (blue). Scale bar 50 μm. Picture representative of 8 clusters from 4 mice in two independent experiments (**e**) Enumeration of the mesenteric clusters of newborns and animals aged between 1 and 32 weeks (n=5, 5, 5, 5, 7, 18, 7, 7 mice per group). Data representative of three independent experiments. Data points and mean shown.

Figure 2. CXCL13 expression by FALC stromal cells is necessary for B cell recruitment.

(**a**) Real-time PCR analysis of the indicated mRNA in LNs, mesenteric FALCs and adjacent fat (n=5, 4, 5). Mann-Whitney nonparametric two-tailed test between FALCs and fat *Cxcl13* p=0.0159, *Tnf* p=0.0286, *Ccl21* p=0.1143, *Ltb* p=0.0079, *Ccl19* p=0.2857, *Il7* p=0.0286. (**b-c**) Numbers of mesenteric clusters in WT, *Plt/plt*, $Ccr7^{-/-}$, and $Cxcr5^{-/-}$ mice (n=7, 6, 6, 6 mice per group), (**b**) and whole mount immunofluorescence staining showing FALCs with $CD11b^+$ myeloid cells (blue), $CD45^+$ hematopoietic cells (green), IgM^+ B cells (red), and $CD4^+$ T cells (white) (**c**) in the indicated mouse strains. Picture representative of 8 clusters from 4 mice from at least 2 independent experiments. (**d**) Whole mount immunofluorescence staining showing mesenteric FALCs in the indicated mouse strains with $CD45^+$ hematopoietic cells (green), and $CXCL13^+$ stromal cells (red). Picture representative of 8 clusters from 4 mice from 2 independent experiments. Scale bar 50 μm. *$p < 0.05$, **$p < 0.01$ and NS not significant.

Figure 3. B cell activation and differentiation in FALCs upon peritoneal immune challenge.

(**a**) Quantification of NP-specific IgM and IgG antibody forming cells (AFC) using ELISpot assays with cells from isolated FALCs and spleens after NP-Ficoll IP immunization of QMxB6 mice. Data correspond to PBS and NP-Ficoll treated mice (n=12,12) pooled from 2 independent experiments using 2.5 x 10^5 cells per well (n=9 FALCs and 12 spleen). Each symbol represents an individual mouse. Mann-Whitney nonparametric two-tailed test between PBS and NP-Ficoll immunised mice, FALCs IgM p=0.0037, spleen IgM p<0.0001, FALCs IgG p=0.0275 and spleen IgG p<0.0001. (**b**) Whole mount immunofluorescence staining of the mesenteries of Cγ1-CrexQMmTmG mice that were immunized with either PBS (all cells red) or NP-Ficoll that results in the generation of $IgG1^+$-switched B cells (green) in FALC. Cγ1-CrexQMmTmG carry one copy of the Cre recombinase in the constant region of the Cγ1 *Igh* gene, one copy of the NP-specific *Igh* from QM mice and the membrane Tomato membrane Green (mTmG) reporter. NP immunization induced B cell activation and Ig class switching with the concomitant expression of Cre recombinase that resulted in the membrane reporter switch from IgM (red) to IgG (green). Arrows indicate the presence of B cells that have undergone switching (green). (**c-d**) Peritoneal lavage cells from QM/QM $EYFP^{+/-}$ mice were transferred by intravenous (IV) injection into C57BL/6J mice 24 hours before immunization with Alum-precipitated NP-OVA. (**c**) Flow cytometric analysis of cells isolated from the mesenteries, spleen and mLN of PBS and NP-OVA-immunized mice showing the percentage of $EYFP^+CD19^+$ NP-specific B cells in live $CD45^+$ gate (top) and percentage of $CD38^-GL7^+$ GC B cells in $EYFP^+CD19^+$ NP-specific B cells gate (bottom). (**d**) Quantification of the cell number of NP-specific B cells (left) and NP-specific GC B cells (right). Data correspond to PBS and NP-OVA treated mice (n=5, 6) pooled from 2 independent experiments. Each symbol represents an individual mouse. Mann-Whitney nonparametric two-tailed test between PBS and NP-OVA treated mice, number of NP^+ B cells/1.10^6 cells in the mesenteries p= 0.0079, spleen p=0.0317, mLN p=0.0079, and number of NP^+ GC B cells/1.10^6 cells in the mesenteries p=0.0043, spleen p=0.0043, mLN p=0.0043. (**e-f**) C57BL/6J mice were immunized IP with Alum precipitated-PE. (**e**) Flow-cytometric analysis of the mesenteries of naïve and PE immunised mice showing percentages of PE^+CD19^+ B cells in live $CD45^+$ gate (upper row), and $CD38^-GL7^+$ GC B cells in PE^+CD19^+ gate (lower row). (**h**) Quantification of the cell number of PE^+ GC B cells. Data correspond to PBS and PE/Alum immunised mice (n=6, 7) pooled from 2 independent experiments. Mann-Whitney nonparametric two-tailed test between PBS and PE/Alum immunised mice, number of PE^+ GC B cells/1.10^6 cells in

the mesenteries p= 0.0043, spleen p=0.0012, mLN p=0.0012 (**h**). *p < 0.05, **p < 0.01, ***p< 0.001 and ****p <0.0001.

Figure 4: Factors controlling the development of FALCs

(**a**) Number of mesenteric clusters in the indicated knockout mouse strains. Data correspond to WT, *Ltbr*$^{-/-}$, *Lta*$^{-/-}$, *Rorc*$^{-/-}$, *Rag2*$^{-/-}$, *Rag2*$^{-/-}$*IL2rg*$^{-/-}$, germ free (GF), *Tnfrsf1a*$^{-/-}$*Tnfrsf1b*$^{-/-}$ and *Tnf*$^{+/\Delta ARE}$ mice pooled from at least 2 independent experiments (n=19, 13, 8, 7, 10, 7, 9, 9, 9 mice per group). Mann-Whitney nonparametric two-tailed test between WT and *Rag2*$^{-/-}$*IL2rg*$^{-/-}$ p< 0.0001, WT and *GF p<0.0001*, WT and *Tnfrsf1a*$^{-/-}$ *Tnfrsf1b*$^{-/-}$ p=0.0002, WT and *Tnf*$^{+/\Delta ARE}$ p<0.0001 (**b**) Whole mount immunofluorescence staining showing FALCs with CD11b^{+} myeloid cells (blue), CD45^{+} hematopoietic cells (green), IgM^{+} B cells (red), and CD4^{+} T cells (white) in the indicated mouse strains. Picture representative of 8 clusters from 4 mice from at least 2 independent experiments. (**c-e**) Microphotographs of the mesenteries of WT mice (**c**), number of clusters (**d**) and whole mount immunofluorescence staining as in b (**e**) after PBS or zymosan injection (n=8, 9). Data pooled from 2 independent experiments. Picture representative of 8 clusters from 4 mice from 2 independent experiments. Mann-Whitney nonparametric two-tailed test p<0.0001. Scale bar 50 µm. *p<0.001 and ** p <0.0001.

Figure 5: TNF is required for FALC formation upon inflammation

(**a**) Number of clusters found in the mesenteries of *Tnfrsf1a*$^{-/-}$*Tnfrsf1b*$^{-/-}$ mice and whole mount immunofluorescence staining showing FALCs with CD11b^{+} myeloid cells (blue), CD45^{+} hematopoietic cells (green), IgM^{+} B cells (red), and CD4^{+} T cells (white) 72 hours after PBS or zymosan injection. Data pooled from 2 independent experiments (n=6, 6). Mann-Whitney nonparametric two-tailed test p=0.2424. Picture representative of 8 clusters from 4 mice from 2 independent experiments. (**b**) Number of clusters present in the mesenteries of WT and *Tnfrsf1a*$^{-/-}$*Tnfrsf1b*$^{-/-}$ mice reconstituted with WT bone marrow and whole mount immunofluorescence staining as in **a** after PBS or zymosan injection. Data correspond to WT BM into WT mice (n=5, 5) and WT BM into *Tnfrsf1a*$^{-/-}$*Tnfrsf1b*$^{-/-}$mice (n=6, 6) per group pooled from 2 independent experiments. Mann-Whitney nonparametric two-tailed test, WT BM into WT mice p=0.0079, and WT BM into *Tnfrsf1a*$^{-/-}$*Tnfrsf1b*$^{-/-}$ mice p=0.1688. Picture representative of 8 clusters from 4 mice from 2 independent experiments. (**c**) Enumeration of clusters in the mesenteries of the indicated mutant mouse strains and whole mount immunofluorescence as in **a** after PBS or zymosan

injection. Data correspond to WT mice (n=7, 7), *T-Tnf*$^{-/-}$ (n=6, 8), *B-Tnf*$^{-/-}$ (n=4, 6) and *M-Tnf*$^{-/-}$ (n=8, 13) mice in the control and treated group pooled from 2 independent experiments. Mann-Whitney nonparametric two-tailed test WT p=0.0006, *T-Tnf*$^{-/-}$ p=0.0007, *B-Tnf*$^{-/-}$ p=0.0048 and *M-Tnf*$^{-/-}$ p=0.2156. Picture representative of 8 clusters from 4 mice from 2 independent experiment. Scale bar 50 µm. Each symbol represents an individual mouse. (**d**) Flow-cytometric analysis showing TNF intra-cellular staining 2 hours post zymosan injection in mesenteric eosinophils (gated as CD45$^+$CD11b$^+$SSC^{high}Siglec-F$^+$), neutrophils (gated as CD45$^+$CD11b$^+$Siglec-F$^-$Ly6-G^{high}), macrophages (gated as CD45$^+$CD11b$^+$Siglec-F$^-$F4/80$^+$) and monocytes (gated as CD45$^+$CD11b$^+$Siglec-F$^-$F4/80$^-$ Ly6-c^{high}). Quantification of the percentages of TNF$^+$ cells after zymosan in myeloid subsets is shown in bar chart. Data correspond to WT mice in the control and treated group (n=8, 8) pooled from 2 independent experiments. Mann-Whitney nonparametric two-tailed test, eosinophils p=0.1593, neutrophils p=0.3935, macrophages p=0.0002 and monocytes p=0.0002. *p < 0.01, **p< 0.001

Figure 6: CD1d restricted NKT cells are required for FALC formation

(**a-b**) Number of mesenteric clusters in the indicated mouse strains (**a**) and whole mount immunofluorescence staining showing FALCs with CD11b$^+$ myeloid cells (blue), CD45$^+$ hematopoietic cells (green), IgM$^+$ B cells (red), and CD4$^+$ T cells (white) 72 hours after PBS or Zymosan injection (**b**). Data correspond to *Rag2*$^{-/-}$ (n=6, 6), *Ighm*$^{-/-}$ (n=5, 5), *Tg(CD3E)26Cpt* (n=5, 5), *Tcrd*$^{-/-}$ (n=4, 6) and *Cd1d*$^{-/-}$ (n=5, 6) mice in the control and treated group pooled from 2 independent experiments. Mann-Whitney nonparametric two-tailed test, *Rag2*$^{-/-}$ p=0.5693, *Ighm*$^{-/-}$ p=0.0025, *Tg(CD3E)26Cpt* p=0.7857, *Tcrd*$^{-/-}$ p=0.0095 and *Cd1d*$^{-/-}$ p=0.5065. Picture representative of 8 clusters from 4 mice from 2 independent experiments. Scale bar 50 µm. *p <0.01, NS not significant.

Figure 7: iNKT cell activation induces FALC formation

(**a**) Flow cytometry of the mesenteries, spleen and mLN showing the percentage of CD3ε$^+$ CD1d-α-GalCer tetramer$^+$ iNKT cells in the lymphocyte gate. Data are representative of 3 independent experiments (**b**) Whole mount immunofluorescence staining showing CFSE loaded iNKT cells (green) in mesenteric FALCs with CD11b$^+$ myeloid cells (blue) and IgM$^+$ B cells (red) 24 hours after transfer. Data representative of 8 clusters from 4 mice in 2 independent experiments. (**c-d**) Numbers of mesenteric clusters and whole mount immunofluorescence staining showing FALCs with CD11b$^+$ myeloid cells (blue), CD45$^+$ hematopoietic cells (green), IgM$^+$ B cells (red), and CD4$^+$ T cells (white) 72 hours after

vehicle or α-GalCer injection. Data correspond to WT mice in the control and treated group (n=6, 9) pooled from 2 independent experiments (**c**) and *Tnfrsf1a*$^{-/-}$*Tnfrsf1b*$^{-/-}$ mice in the control and treated group (n=9, 7) pooled from 3 independent experiments. Picture representative of 8 clusters from 4 mice from at least 2 independent experiments (**d**). Mann-Whitney nonparametric two-tailed test, WT p=0.0004 and *Tnfrsf1a*$^{-/-}$*Tnfrsf1b*$^{-/-}$ p=0.2831. (**e**) Numbers of mesenteric clusters and whole mount immunofluorescence staining showing FALCs with CD11b^{+} myeloid cells (blue) and CD45^{+} hematopoietic cells (green) 72 hours after PBS or zymosan injection in *Rag2*$^{-/-}$ mice (n=4, 5) and *Rag2*$^{-/-}$ mice transferred with high purity sorted CD3^{high} T cells or CD3ε^{+} CD1d-α-GalCer tetramer^{+} iNKT cells (n=6, 5). Data pooled from 4 independent experiments. Mann-Whitney nonparametric two-tailed test p=0.0043. Picture representative of 8 clusters from 4 mice from 4 independent experiments. (**f**) Numbers of mesenteric clusters in *Tcra-Jα18*$^{-/-}$ mice and whole mount immunofluorescence as in **c** 72 hours after PBS or zymosan injection (n=7, 6). Data correspond pooled from 2 independent experiments. Mann-Whitney nonparametric two-tailed test p=0.0012. Picture representative of 8 clusters from 4 mice from 2 independent experiments. Scale bar 50 µm. *$p < 0.01$, **$p< 0.001$ and NS not significant.

Figure 8: Formation of FALCs is dependant on IL-4Rα signaling

(**a-b**) Numbers of mesenteric clusters in the indicated mouse strains (**a**) and whole mount immunofluorescence staining showing FALCs with CD11b^{+} myeloid cells (blue), CD45^{+} hematopoietic cells (green), IgM^{+} B cells (red), and CD4^{+} T cells (white) 72 hours after PBS or Zymosan injection. Data correspond to WT (n=7, 6), *Il4ra*$^{-/-}$ (n=5, 5), *Il4*$^{-/-}$ (n=5, 6), and *Il13*$^{-/-}$ mice (n=4, 6) in the control and treated group pooled from 2 independent experiments. Mann-Whitney nonparametric two-tailed test, WT p=0.0012, *Il4ra*$^{-/-}$ p=0.8016, *Il4*$^{-/-}$ p=0.0043, and *Il13*$^{-/-}$ mice p=0.0095. Picture representative of 8 clusters from 4 mice from 2 independent experiments. Scale bar 50 µm. (**c**) Numbers of mesenteric clusters in *Il13*$^{-/-}$ mice and *Il13*$^{-/-}$ mice transferred with high purity sorted CD1d-α-GalCer tetramer^{+} iNKT cells or CD3^{high} T cells 72 hours after PBS or zymosan injection. Data correspond to *Il13*$^{-/-}$ control injected with PBS (n=7), injected with zymosan (n=6), received CD3^{high} T cells and was injected with zymosan (n=6) and received iNKT cells and was injected with zymosan (n=6) pooled from 2 independent experiments. Mann-Whitney nonparametric two-tailed test p=0.3625. (**d**) Numbers of mesenteric clusters in C57Bl/6J and *Il4ra*$^{-/-}$ mice 72 hours after PBS or zymosan injection. Data correspond to

WT control (n=9) and treated (n=5) and *Il4ra*$^{-/-}$ control (n=7) and treated (n=5) pooled from 2 independent experiments. Mann-Whitney nonparametric two-tailed test, WT p=0.001 and *Il4ra*$^{-/-}$ p=0.2159. **p* < 0.01, ***p*< 0.001 and NS not significant.

METHODS

Mice

C57BL/6J (H-2^b), *Ltbr*$^{-/-}$, *Lta*$^{-/-}$, *Rorc*$^{-/-}$, *Rag2*$^{-/-}$, *Rag2*$^{-/-}\gamma c^{-/-}$, *Tnfrsf1a*$^{-/-}$ *Tnfrsf1b*$^{-/-}$, *Tnf*$^{+/\Delta ARE50}$, and *Eyfp-Rosa26*, *Plt/plt*, *Ccr7*$^{-/-}$, *Cxcr5*$^{-/-}$, QM/QM (Igh-J$^{tm1(VDJ-17.2.25)Wabl}$)[36] (*Igh*$^{NP/NP}$ *Igk*$^{-/-}$), QM × B6 (*Igh*$^{NP/+}$ *Igk*$^{+/-}$), QM/QM EYFP$^+$ (QM-EYFP$^+$), Cγ1-CrexQMmTmG (Gt(ROSA)26Sor$^{tm4(ACTB-tdTomato,-EGFP)Luo}$)(*Igh*$^{NP/C_\gamma 1Cre}$ *Igk*$^{-/-}$)[51,52], Tg(CD3E)26Cpt, *Cd1d*$^{-/-}$, *Tnf*$^{fl/fl}$*Lysm*-Cre (M-TNF)[53], *Tnf*$^{fl/fl}$*Cd4*-Cre (T-TNF)[53] or *Tnf*$^{fl/fl}$*Cd19*-Cre (B-TNF)[53], *Tcra-Jα18*$^{-/-}$, Vα14-Jα18 Tg, *Ifng*$^{-/-}$, *Il13*$^{-/-}$ (on C57BL/6J background), *Il4*$^{-/-}$, *Il4ra*$^{-/-}$, *Il13*$^{-/-}$ (on BALB/c background) and BALB/c (H-2^d) mice were bred and maintained under specific pathogen-free conditions. *Il13*$^{-/-}$*, and Il4ra*$^{-/-}$ mice were used in C57BL/6J or BALB/c background for experiments as indicated. Germ-free C57BL/6J mice were obtained from the Institut Pasteur, Paris, France. Bone marrow chimeras were generated after irradiation of C57BL/6J and *Tnfrsf1a*$^{-/-}$*Tnfrsf1b*$^{-/-}$, mice and reconstitution with bone marrow from C57BL/6J. All experiments in this report were performed according to UK Home Office and local ethics committee regulations.

Immunization and peritoneal cavity inflammation

QM/QM (*Igh*$^{NP/NP}$ *Igk*$^{-/-}$), QM × B6 (*Igh*$^{NP/+}$ *Igk*$^{+/-}$), and Cγ1-CrexQMmTmG mice were immunized by intraperitoneal injection of 30 μg NP40-Ficoll per mouse (Biosearch Technologies). B cell activation from mesenteries, spleen, mLN and peritoneal cavity lavage was assessed 24 h later (QM/QM mice) or 4 d later (QM × B6 and Cγ1-CrexQMmTmG mice) by flow cytometry and ELISPOT. IgG1 switching in the mesenteries was visualized at day 4 by whole-mount stereo-microscopy. For cell transfer experiments, 2 × 10^6 peritoneal lavage cells from QM-EYFP$^+$ mice were transferred IP into recipient C57BL/6J mice, before immunization with NP-OVA (50 μg) precipitated with Alum on the next day. B cell activation was assessed at day 8 in the mesenteries, spleen and mLN. For the PE immunization experiment, C57BL/6J mice were immunized IP with Phycoerythrin (PE) (50 μg) and B cell activation was analyzed at day 8-9 in the mesenteries, spleen and mLN. Peritoneal cavity inflammation was induced by Intraperitoneal injection of 1 mg Zymosan (Sigma). 72 h later, B cell activation was assessed by flow cytometry, FALC number and composition were assessed by whole mount fluorescence staining and confocal analysis. Treatment of mice with IL-4c was performed as previously described[54]. IL-4c consisted of a 2:1 molar ratio of recombinant mouse IL-4 (Peprotech) and anti-IL-4

mAb (clone 11B11;BioXcell). Mice were injected i.p. with IL-4c containing 5 μg of IL-4 and 25 μg of 11B11, or PBS vehicle control on days 0 and 2. For co-administration experiments with Zymosan, mice were given 1 mg Zymosan on day 0 with IL-4c on day 0 and day 2. Mice were treated with 1 μg TNF (Peprotech) or PBS control on day 0 and day 2. For co-administration experiment with IL-4c, mice were treated with IL-4c and TNF on day 0 and day 4. For co-administration experiment with Zymosan, mice were given 1 mg Zymosan on day 0 and TNF on day 0 and day 2. In all experiments with IL-4c and TNF, analysis of the mesenteries was performed on day 4.

Cell isolation and cell sorting

For flow cytometric analysis of the mesenteries, tissues were digested for 30 min in RPMI containing 1% fetal calf serum and 1 mg/ml Collagenase D (Roche) at 37 °C on constant agitation (110 r.p.m.). Tissue suspensions were filtered was filtered through 40 μm cell strainers before staining. Peritoneal cavity lavage was performed by injection of 5 ml cold PBS in the peritoneal cavity. Isolation of splenic $CD3\varepsilon^{low}$ CD1d-PBS-57 $Tetramer^{+}$ *i*NKT cells and $CD3\varepsilon^{hi}$ T cells was performed via MoFlow (Dako Cytomation) cell sorting. 5×10^5 cells (purity> 98%) were injected in the peritoneal cavity of *Rag2*$^{-/-}$, 12 h before induction of peritoneal cavity inflammation. Mesenteries were analyzed for cluster formation 72 h later. For CFSE labeling, *i*NKT cells were isolated by high speed cell sorting from the spleen of $V_\alpha 14$ transgenic mice in which 30–40% of all cells are positive for α-GalCer-loaded CD1d tetramers and were incubated for 10 min at 22°C with 5 μM CFSE (eBiosciences) according to manufacturer indications prior to intraperitoneal injection. CD1d-PBS57 loaded tetramers were kindly provided by the National Institutes of Health Tetramer Facility (Atlanta GA, USA).

Antibodies and reagents for flow cytometry

Antibodies and reagents used for flow cytometry are listed in **Supplementary Table 1**. Single-cell suspensions were stained with primary conjugated antibodies followed by secondary antibodies. NP-specific B cells were detected with NP-PE, added with the primary antibody staining mix. *i*NKT cells were detected with CD1d tetramer conjugated with APC preloaded with PBS-57 (an analog of α-GalCer). CD1d-PBS-57-APC was also added to the primary antibody staining mix. For Ki67 nuclear staining, cells were fixed and permeabilized with the Foxp3 Fixation/Permeabilization kit (eBiosciences). Flow cytometric analysis was performed using Cyan (BD Biosciences) with forward/side scatter gates set

to exclude non-viable cells. Data were analyzed with FlowJo software (version 8.8.3, Tree Star).

FALC isolation

Clusters were isolated using a fluorescent stereomicroscope from unfixed mesenteries of $EYFP^+$ mice in which the bright $EYFP^+$ lymphoid aggregates could be visualized without prior fluorescent staining. Isolated clusters were used for qPCR analysis.

ELISPOT assays.

2.5×10^5 cells from the mesenteries or spleen were seeded into precoated NP_{15}-BSA (5 μg/ml)- nitrocellulose microtiter plates. After 24 h culture the plates were washed and incubated in isotype specific alkaline phosphatase-conjugated antibody IgM-AP1/ IgG-AP1 (SouthernBiotech) diluted in PBS-1%BSA for 2 h at 22°C and developed using Fast BCIP/NBT alkaline phosphatase substrate (Sigma). Spots were counted using an AID ELISpot reader (Autoimmun Diagnostika GmbH) with Eli4 software (Autoimmun Diagnostika GmbH).

RT-PCR and real-time RT-PCR

mRNAs were isolated from tissues using the RNeasy mini kit (Qiagen), and reverse transcription was performed using the High capacity reverse transcription cDNA synthesis kit (Applied Biosystems). Quantitative RT-PCR was performed using primers and probes from Applied Biosystems for *Cxcl13* (Mm00444533_m1), *Ccl21* (Mm03646971_gH), *Ccl19* (Mm00839967_g1), *Tnf* (Mm00443258_m1), *Ltb* (Mm00434774_g1) and *Il7* (Mm01295803_m1) using ABI PRISM 7900HT instrument. The means of duplicate of the ratio of the gene of interest to *Actb* are shown.

Immunofluorescence staining

After dissection, whole mesenteries were fixed in PBS 4%PFA for 1 h at 4 °C, permeabilized in PBS 1%Triton for 30 min at 22°C. Tissues were then stained with primary antibodies for 1 h at 22°C on constant slow agitation. After wash, tissues were stained with secondary antibodies for 30 min at 22°C. Antibodies used are listed in **Supplementary Table 1**. Tissues were mounted using Vectashield mounting medium (Vector Laboratories).

Image acquisition and analysis of confocal images

Confocal images were acquired using a Zeiss LSM 510 laser scanning confocal head with a Zeiss Axio Imager Z1 microscope. For all analysis of clusters a minimum of 12 clusters were analysed from 4 mice of each group and pooled from 2 independent experiments.

Statistical analysis

Statistical significance was determined for all analysis with a Mann-Whitney non parametric two-tailed test.

REFERENCES

1. Silverman, G.J., Gronwall, C., Vas, J. & Chen, Y. Natural autoantibodies to apoptotic cell membranes regulate fundamental innate immune functions and suppress inflammation. *Discov Med* **8**, 151-156 (2009).
2. Alugupalli, K.R. *et al.* B1b lymphocytes confer T cell-independent long-lasting immunity. *Immunity* **21**, 379-390 (2004).
3. Ochsenbein, A.F. *et al.* Control of early viral and bacterial distribution and disease by natural antibodies. *Science* **286**, 2156-2159 (1999).
4. Baumgarth, N. *et al.* B-1 and B-2 cell-derived immunoglobulin M antibodies are nonredundant components of the protective response to influenza virus infection. *J Exp Med* **192**, 271-280 (2000).
5. Haas, K.M., Poe, J.C., Steeber, D.A. & Tedder, T.F. B-1a and B-1b cells exhibit distinct developmental requirements and have unique functional roles in innate and adaptive immunity to S. pneumoniae. *Immunity* **23**, 7-18 (2005).
6. Boes, M., Prodeus, A.P., Schmidt, T., Carroll, M.C. & Chen, J. A critical role of natural immunoglobulin M in immediate defense against systemic bacterial infection. *J Exp Med* **188**, 2381-2386 (1998).
7. Martin, F., Oliver, A.M. & Kearney, J.F. Marginal zone and B1 B cells unite in the early response against T-independent blood-borne particulate antigens. *Immunity* **14**, 617-629 (2001).
8. Platell, C., Cooper, D., Papadimitriou, J.M. & Hall, J.C. The omentum. *World J Gastroenterol* **6**, 169-176 (2000).
9. Ansel, K.M., Harris, R.B. & Cyster, J.G. CXCL13 is required for B1 cell homing, natural antibody production, and body cavity immunity. *Immunity* **16**, 67-76 (2002).
10. Carlow, D.A., Gold, M.R. & Ziltener, H.J. Lymphocytes in the peritoneum home to the omentum and are activated by resident dendritic cells. *J Immunol* **183**, 1155-1165 (2009).
11. Ha, S.A. *et al.* Regulation of B1 cell migration by signals through Toll-like receptors. *J Exp Med* **203**, 2541-2550 (2006).
12. Rangel-Moreno, J. *et al.* Omental milky spots develop in the absence of lymphoid tissue-inducer cells and support B and T cell responses to peritoneal antigens. *Immunity* **30**, 731-743 (2009).

13. Elewa, Y.H., Ichii, O., Otsuka, S., Hashimoto, Y. & Kon, Y. Characterization of mouse mediastinal fat-associated lymphoid clusters. *Cell Tissue Res* **357**, 731-41 (2014).
14. Moro, K. *et al.* Innate production of T(H)2 cytokines by adipose tissue-associated c-Kit(+)Sca-1(+) lymphoid cells. *Nature* **463**, 540-544 (2010).
15. Price, A.E. *et al.* Systemically dispersed innate IL-13-expressing cells in type 2 immunity. *Proc Natl Acad Sci U S A* **107**, 11489-11494 (2010).
16. Neill, D.R. *et al.* Nuocytes represent a new innate effector leukocyte that mediates type-2 immunity. *Nature* **464**, 1367-1370 (2010).
17. Spits, H. *et al.* Innate lymphoid cells--a proposal for uniform nomenclature. *Nat Rev Immunol* **13**, 145-149 (2013).
18. Randall, T.D., Carragher, D.M. & Rangel-Moreno, J. Development of secondary lymphoid organs. *Annu Rev Immunol* **26**, 627-650 (2008).
19. Roozendaal, R. & Mebius, R.E. Stromal cell-immune cell interactions. *Annu Rev Immunol* **29**, 23-43 (2011).
20. Ruddle, N.H. & Akirav, E.M. Secondary lymphoid organs: responding to genetic and environmental cues in ontogeny and the immune response. *J Immunol* **183**, 2205-2212 (2009).
21. Ngo, V.N. *et al.* Lymphotoxin alpha/beta and tumor necrosis factor are required for stromal cell expression of homing chemokines in B and T cell areas of the spleen. *J Exp Med* **189**, 403-412 (1999).
22. Krautler, N.J. *et al.* Follicular dendritic cells emerge from ubiquitous perivascular precursors. *Cell* **150**, 194-206 (2012).
23. Matsumoto, M. *et al.* Distinct roles of lymphotoxin alpha and the type I tumor necrosis factor (TNF) receptor in the establishment of follicular dendritic cells from non-bone marrow-derived cells. *J Exp Med* **186**, 1997-2004 (1997).
24. Ansel, K.M. *et al.* A chemokine-driven positive feedback loop organizes lymphoid follicles. *Nature* **406**, 309-314 (2000).
25. Fu, Y.X., Huang, G., Wang, Y. & Chaplin, D.D. B lymphocytes induce the formation of follicular dendritic cell clusters in a lymphotoxin alpha-dependent fashion. *J Exp Med* **187**, 1009-1018 (1998).
26. Yang, Y. *et al.* Antigen-specific memory in B-1a and its relationship to natural immunity. *Proc Natl Acad Sci U S A* **109**, 5388-5393 (2012).
27. Yang, Y. *et al.* Antigen-specific antibody responses in B-1a and their relationship to natural immunity. *Proc Natl Acad Sci U S A* **109**, 5382-5387 (2012).

28. Brennan, P.J., Brigl, M. & Brenner, M.B. Invariant natural killer T cells: an innate activation scheme linked to diverse effector functions. *Nat Rev Immunol* **13**, 101-117 (2013).
29. Marshall, J.L. *et al.* The capsular polysaccharide Vi from Salmonella typhi is a B1b antigen. *J Immunol* **189**, 5527-5532 (2012).
30. Gil-Cruz, C. *et al.* The porin OmpD from nontyphoidal Salmonella is a key target for a protective B1b cell antibody response. *Proc Natl Acad Sci U S A* **106**, 9803-9808 (2009).
31. Foote, J.B. & Kearney, J.F. Generation of B cell memory to the bacterial polysaccharide alpha-1,3 dextran. *J Immunol* **183**, 6359-6368 (2009).
32. Cascalho, M., Ma, A., Lee, S., Masat, L. & Wabl, M. A quasi-monoclonal mouse. *Science* **272**, 1649-1652 (1996).
33. Marshall, J.L. *et al.* Early B blasts acquire a capacity for Ig class switch recombination that is lost as they become plasmablasts. *Eur J Immunol* **41**, 3506-3512 (2011).
34. De Togni, P. *et al.* Abnormal development of peripheral lymphoid organs in mice deficient in lymphotoxin. *Science* **264**, 703-707 (1994).
35. Futterer, A., Mink, K., Luz, A., Kosco-Vilbois, M.H. & Pfeffer, K. The lymphotoxin beta receptor controls organogenesis and affinity maturation in peripheral lymphoid tissues. *Immunity* **9**, 59-70 (1998).
36. Sun, Z. *et al.* Requirement for RORgamma in thymocyte survival and lymphoid organ development. *Science* **288**, 2369-2373 (2000).
37. Koni, P.A. & Flavell, R.A. A role for tumor necrosis factor receptor type 1 in gut-associated lymphoid tissue development: genetic evidence of synergism with lymphotoxin beta. *J Exp Med* **187**, 1977-1983 (1998).
38. Pabst, O. *et al.* Adaptation of solitary intestinal lymphoid tissue in response to microbiota and chemokine receptor CCR7 signaling. *J Immunol* **177**, 6824-6832 (2006).
39. Bouskra, D. *et al.* Lymphoid tissue genesis induced by commensals through NOD1 regulates intestinal homeostasis. *Nature* **456**, 507-510 (2008).
40. Hamada, H. *et al.* Identification of multiple isolated lymphoid follicles on the antimesenteric wall of the mouse small intestine. *J Immunol* **168**, 57-64 (2002).
41. Kamada, N., Seo, S.U., Chen, G.Y. & Nunez, G. Role of the gut microbiota in immunity and inflammatory disease. *Nat Rev Immunol* **13**, 321-335 (2013).

42. Ji, Y. *et al.* Short Term High Fat Diet Challenge Promotes Alternative Macrophage Polarization in Adipose Tissue via Natural Killer T Cells and Interleukin-4. *J Biol Chem* **287**, 24378-24386 (2012).
43. Ji, Y. *et al.* Activation of natural killer T cells promotes M2 Macrophage polarization in adipose tissue and improves systemic glucose tolerance via interleukin-4 (IL-4)/STAT6 protein signaling axis in obesity. *J Biol Chem* **287**, 13561-13571 (2012).
44. Lynch, L. *et al.* Adipose tissue invariant NKT cells protect against diet-induced obesity and metabolic disorder through regulatory cytokine production. *Immunity* **37**, 574-587 (2012).
45. Schipper, H.S. *et al.* Natural killer T cells in adipose tissue prevent insulin resistance. *J Clin Invest* **122**, 3343-3354 (2012).
46. Wu, L. *et al.* Activation of invariant natural killer T cells by lipid excess promotes tissue inflammation, insulin resistance, and hepatic steatosis in obese mice. *Proc Natl Acad Sci U S A* **109**, E1143-1152 (2012).
47. Fukuyama, S. *et al.* Initiation of NALT organogenesis is independent of the IL-7R, LTbetaR, and NIK signaling pathways but requires the Id2 gene and CD3(-)CD4(+)CD45(+) cells. *Immunity* **17**, 31-40 (2002).
48. Benezech, C. *et al.* Lymphotoxin-beta receptor signaling through NF-kappaB2-RelB pathway reprograms adipocyte precursors as lymph node stromal cells. *Immunity.* **37**, 721-734 (2012).
49. Gil-Ortega, M. *et al.* Native adipose stromal cells egress from adipose tissue in vivo: evidence during lymph node activation. *Stem Cells* **31**, 1309-1320 (2013).
50. Kontoyiannis, D., Pasparakis, M., Pizarro, T.T., Cominelli, F. & Kollias, G. Impaired on/off regulation of TNF biosynthesis in mice lacking TNF AU-rich elements: implications for joint and gut-associated immunopathologies. *Immunity* **10**, 387-398 (1999).
51. Casola, S. *et al.* Tracking germinal center B cells expressing germ-line immunoglobulin gamma1 transcripts by conditional gene targeting. *Proc Natl Acad Sci U S A* **103**, 7396-7401 (2006).
52. Muzumdar, M.D., Tasic, B., Miyamichi, K., Li, L. & Luo, L. A global double-fluorescent Cre reporter mouse. *Genesis* **45**, 593-605 (2007).
53. Grivennikov, S.I. *et al.* Distinct and nonredundant in vivo functions of TNF produced by t cells and macrophages/neutrophils: protective and deleterious effects. *Immunity* **22**, 93-104 (2005).

54. Jenkins, S.J. *et al.* Local macrophage proliferation, rather than recruitment from the blood, is a signature of TH2 inflammation. *Science* **332**, 1284-1288 (2011).

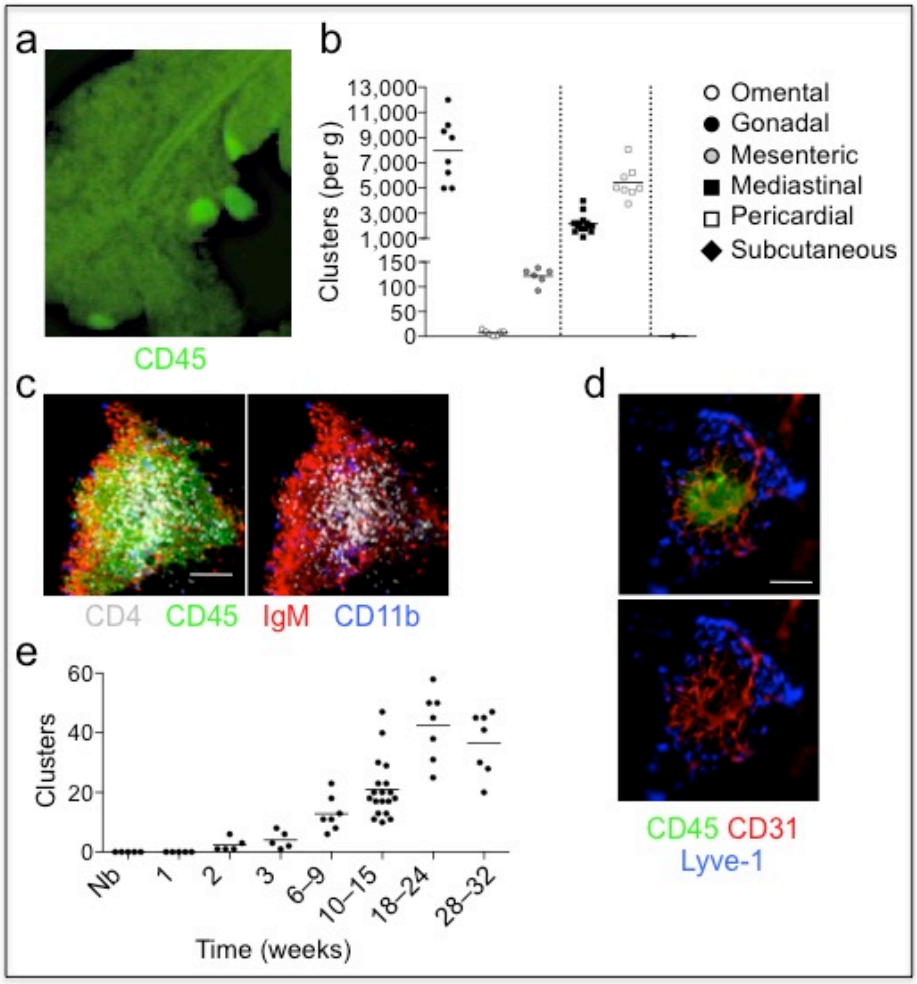
a
CD45
b
Clusters (per g)
13,000
11,000
9,000
7,000
5,000
3,000
1,000
150
100
50
0
Omental
Gonadal
Mesenteric
Mediastinal
Pericardial
Subcutaneous
c
CD4 CD45 IgM CD11b
d
CD45 CD31
Lyve-1
e
Clusters
60
40
20
0
Nb
1
2
3
6–9
10–15
18–24
28–32
Time (weeks)

Figure 1

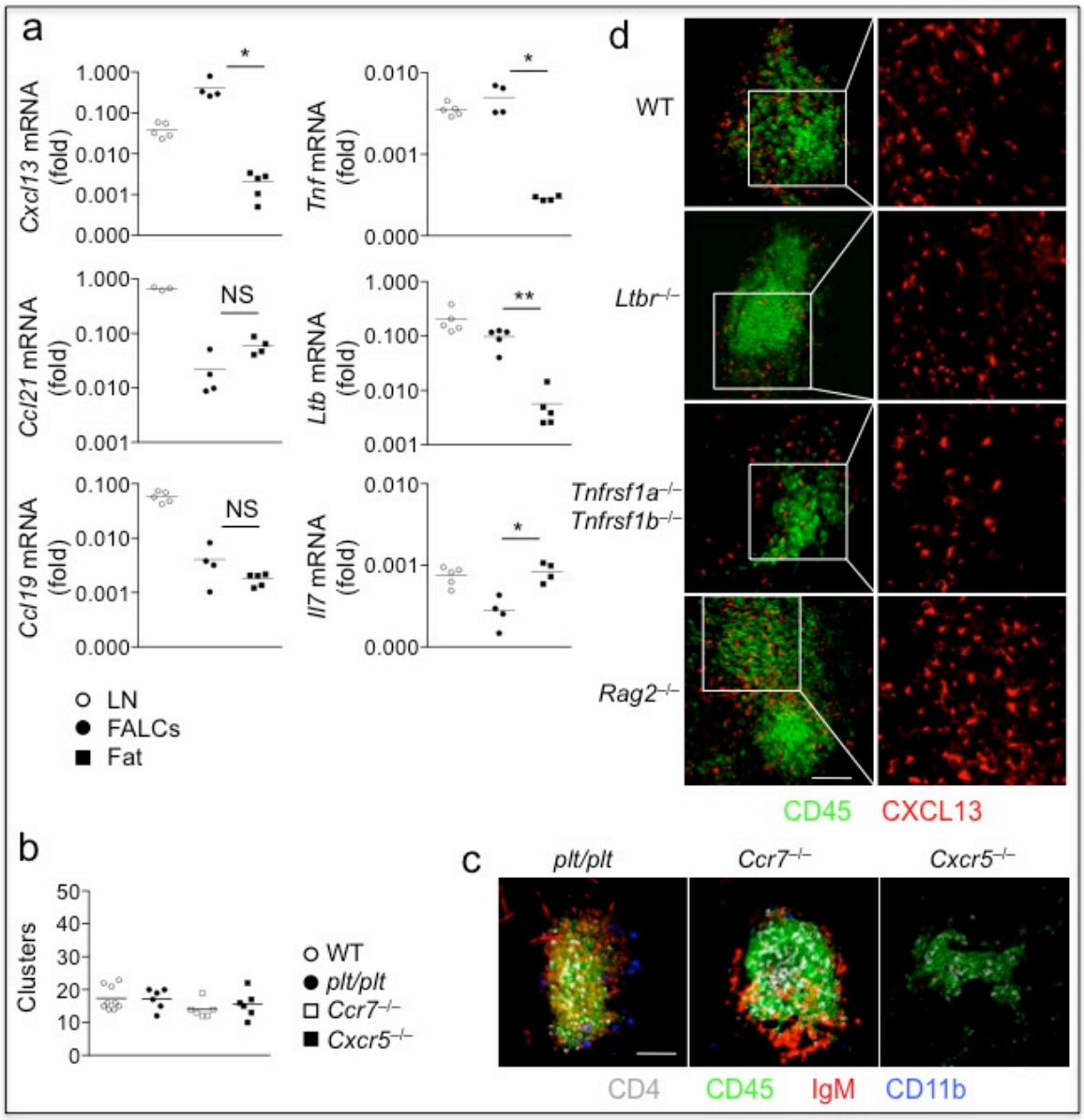
a
Cxcl13 mRNA (fold)
1.000
0.100
0.010
0.001
0.000
*
Tnf mRNA (fold)
0.010
0.001
0.000
*
Ccl21 mRNA (fold)
1.000
0.100
0.010
0.001
NS
Ltb mRNA (fold)
1.000
0.100
0.010
0.001
**
Ccl19 mRNA (fold)
0.100
0.010
0.001
0.000
NS
Il7 mRNA (fold)
0.010
0.001
0.000
*
LN
FALCs
Fat
b
Clusters
50
40
30
20
10
0
WT
plt/plt
Ccr7−/−
Cxcr5−/−
c
plt/plt
Ccr7−/−
Cxcr5−/−
CD4
CD45
IgM
CD11b
d
WT
Ltbr−/−
Tnfrsf1a−/−
Tnfrsf1b−/−
Rag2−/−
CD45
CXCL13

Figure 2

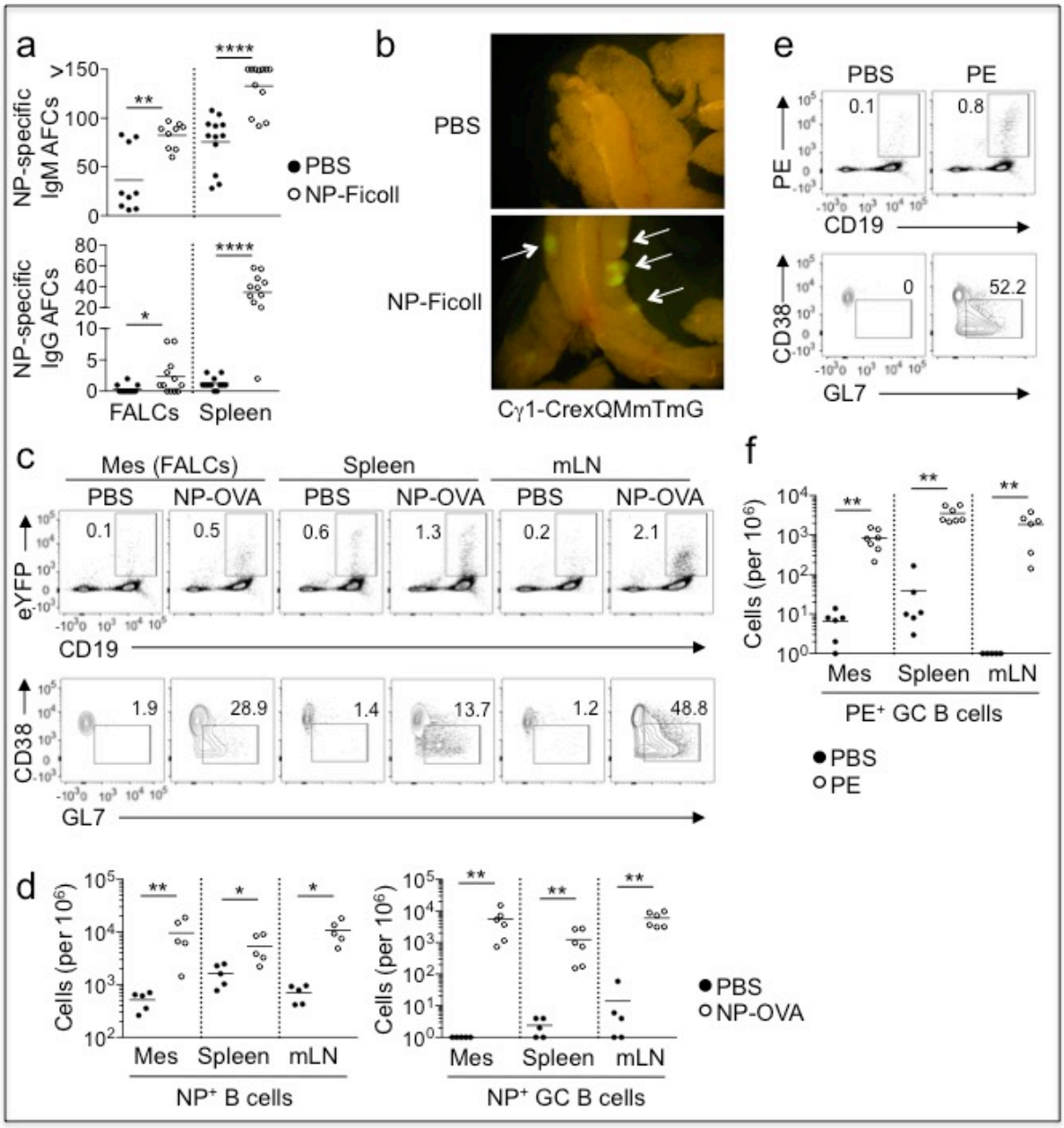
a
NP-specific IgM AFCs
NP-specific IgG AFCs
PBS
NP-Ficoll
FALCs
Spleen
b
PBS
NP-Ficoll
Cγ1-CrexQMmTmG
e
PBS
PE
CD19
CD38
GL7
c
Mes (FALCs)
Spleen
mLN
PBS
NP-OVA
eYFP
CD19
CD38
GL7
d
Cells (per 10^6)
Mes
Spleen
mLN
NP+ B cells
NP+ GC B cells
PBS
NP-OVA
f
PE+ GC B cells
PBS
PE

Figure 3

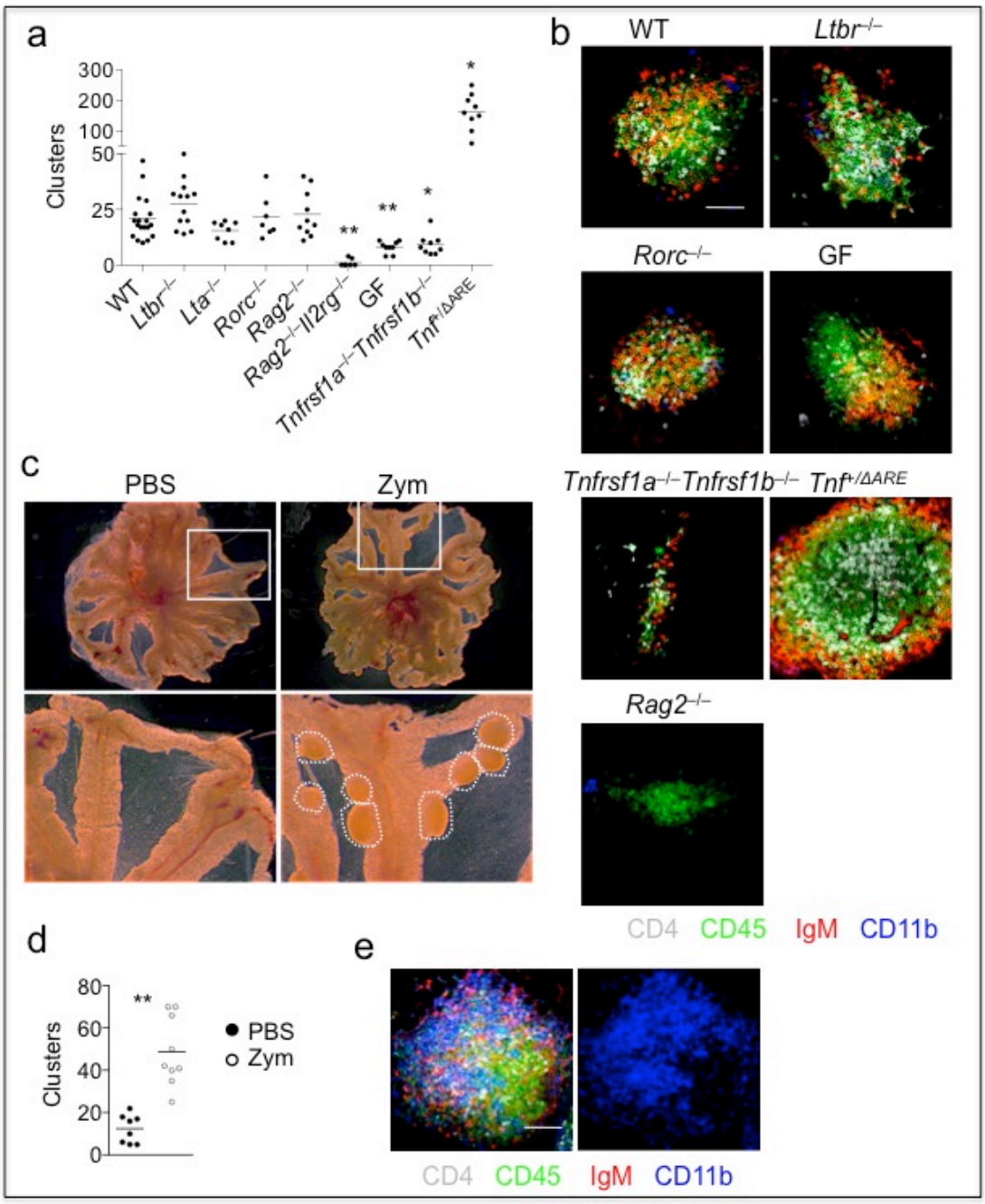
a
Clusters
300
200
100
50
25
0
WT
Ltbr−/−
Lta−/−
Rorc−/−
Rag2−/−
Rag2−/−Il2rg−/−
GF
Tnfrsf1a−/−Tnfrsf1b−/−
Tnf+/ΔARE
b
WT
Ltbr−/−
Rorc−/−
GF
Tnfrsf1a−/−Tnfrsf1b−/−
Tnf+/ΔARE
Rag2−/−
CD4 CD45 IgM CD11b
c
PBS
Zym
d
Clusters
80
60
40
20
0
PBS
Zym
e
CD4 CD45 IgM CD11b

Figure 4

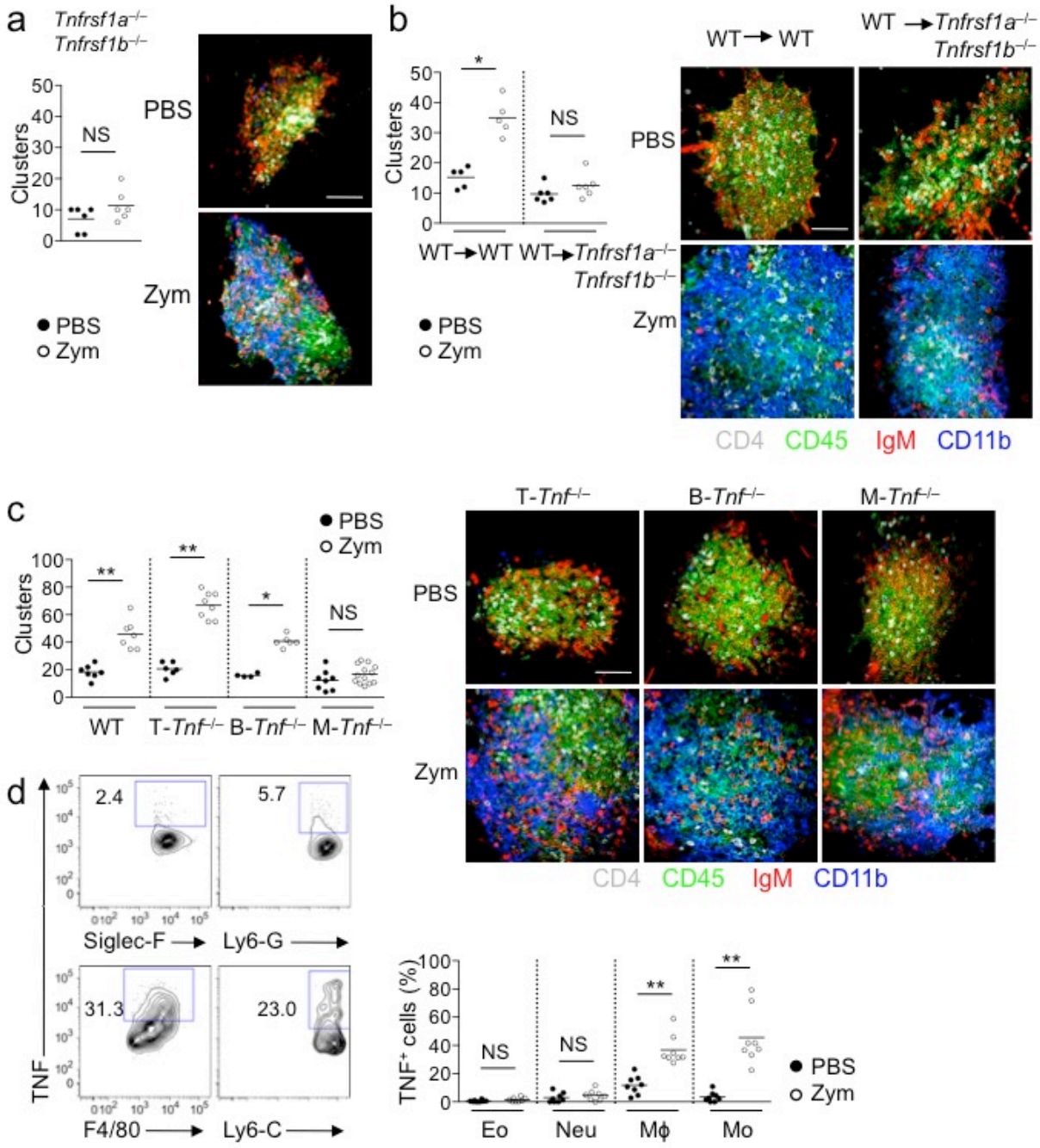
a
Tnfrsf1a−/−
Tnfrsf1b−/−
Clusters
NS
PBS
Zym
● PBS
○ Zym
b
WT → WT
WT → Tnfrsf1a−/−
Tnfrsf1b−/−
*
NS
WT→WT WT→Tnfrsf1a−/−
Tnfrsf1b−/−
PBS
Zym
CD4 CD45 IgM CD11b
c
● PBS
○ Zym
**
*
NS
WT T-Tnf−/− B-Tnf−/− M-Tnf−/−
T-Tnf−/−
B-Tnf−/−
M-Tnf−/−
d
2.4
5.7
31.3
23.0
Siglec-F
Ly6-G
F4/80
Ly6-C
TNF
TNF+ cells (%)
Eo
Neu
Mϕ
Mo

Figure 5

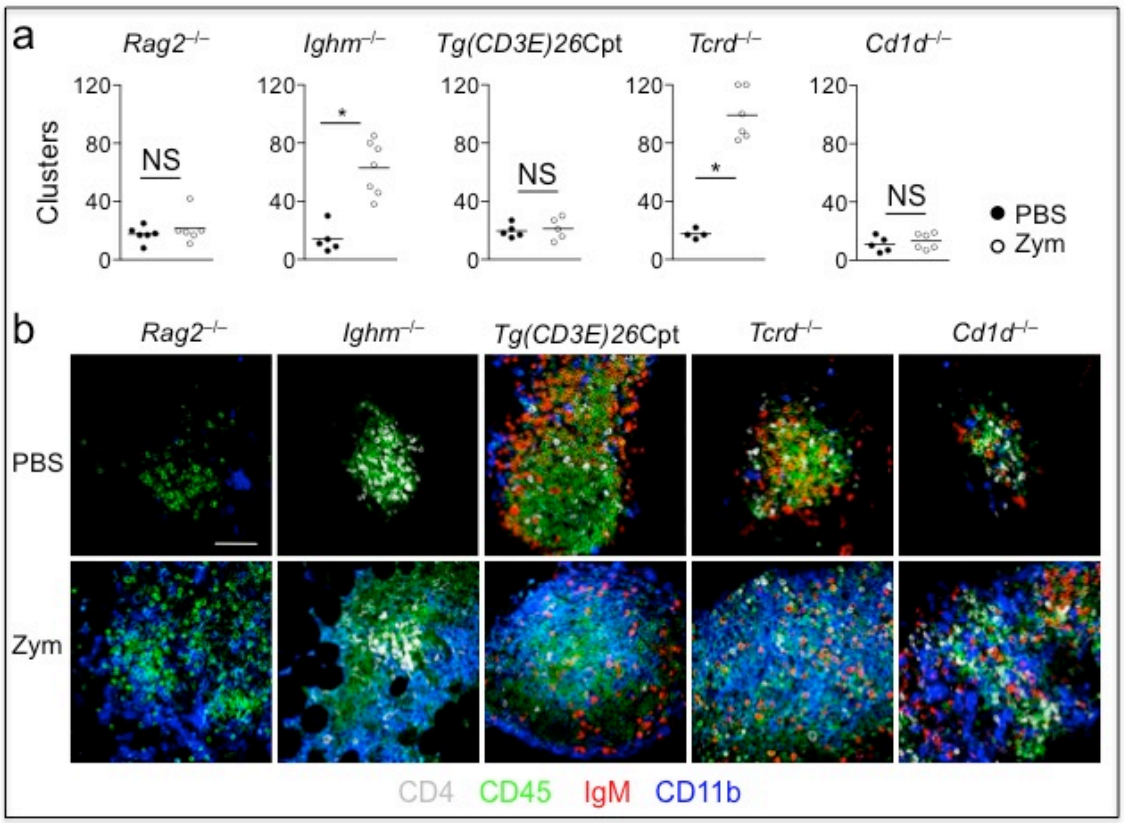
a
Rag2−/−
Ighm−/−
Tg(CD3E)26Cpt
Tcrd−/−
Cd1d−/−
Clusters
120
80
40
0
NS
*
PBS
Zym
b
PBS
Zym
CD4 CD45 IgM CD11b

Figure 6

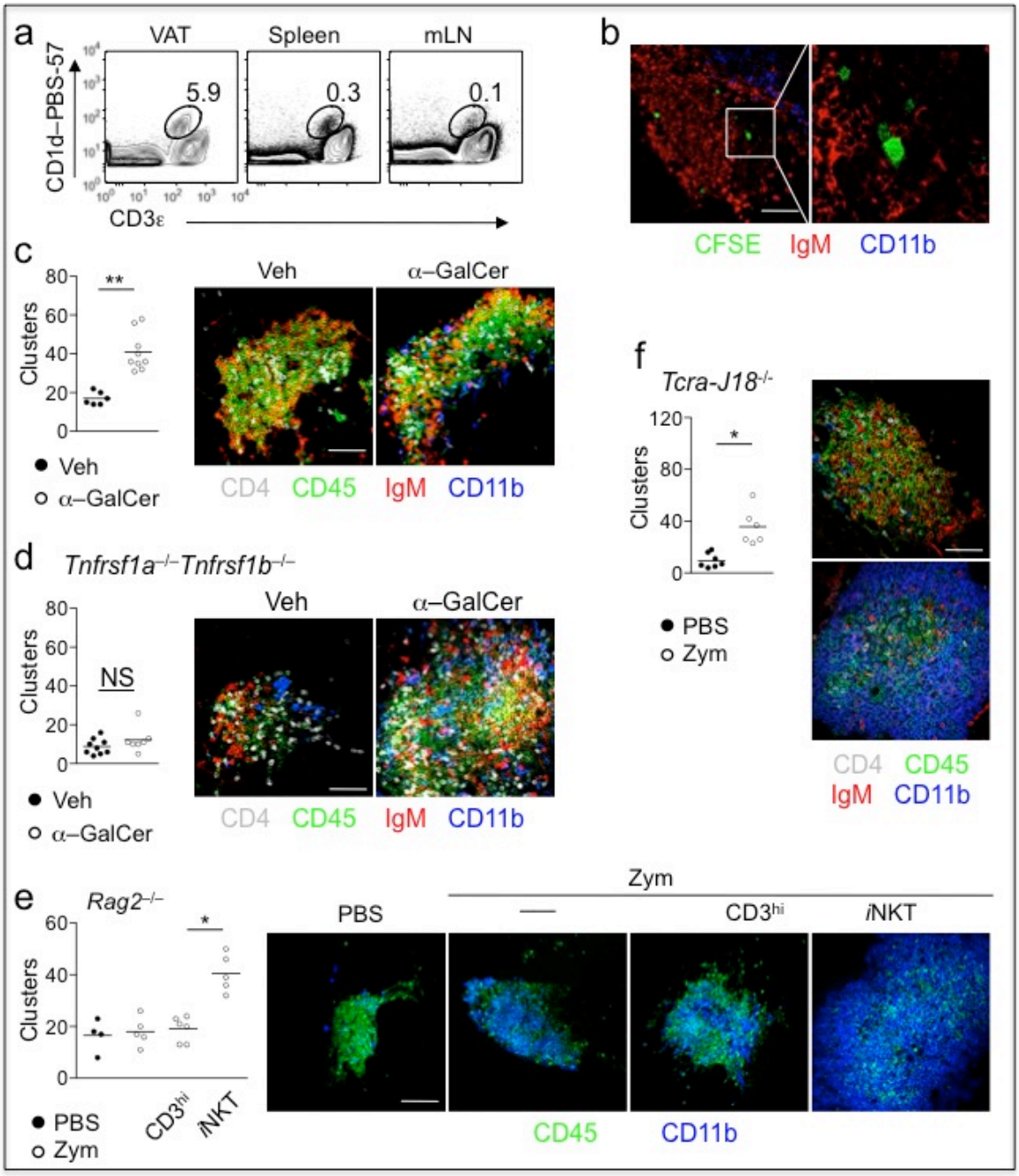
a
VAT
Spleen
mLN
CD1d–PBS-57
CD3ε
5.9
0.3
0.1
b
CFSE IgM CD11b
c
Clusters
**
Veh
α–GalCer
Veh
α–GalCer
CD4 CD45 IgM CD11b
d
Tnfrsf1a−/−Tnfrsf1b−/−
NS
Veh
α–GalCer
CD4 CD45 IgM CD11b
e
Rag2−/−
*
PBS
Zym
CD3hi
iNKT
CD45 CD11b
f
Tcra-J18-/-
*
PBS
Zym
CD4 CD45
IgM CD11b

Figure 7

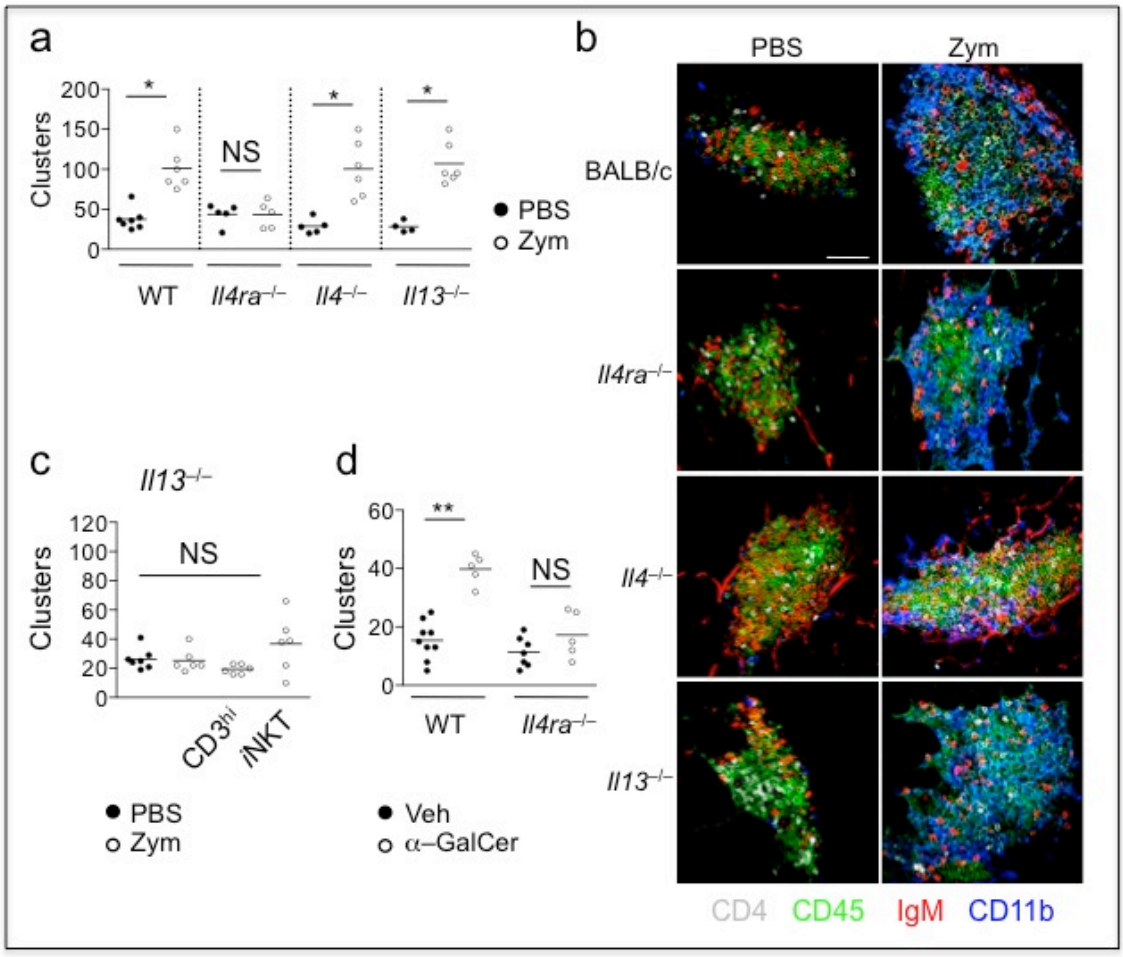
a
Clusters
200
150
100
50
0
*
NS
*
*
PBS
Zym
WT
Il4ra−/−
Il4−/−
Il13−/−
b
PBS
Zym
BALB/c
Il4ra−/−
Il4−/−
Il13−/−
CD4
CD45
IgM
CD11b
c
Il13−/−
Clusters
120
100
80
60
40
20
0
NS
CD3hi
iNKT
PBS
Zym
d
Clusters
60
40
20
0
**
NS
WT
Il4ra−/−
Veh
α–GalCer

Figure 8

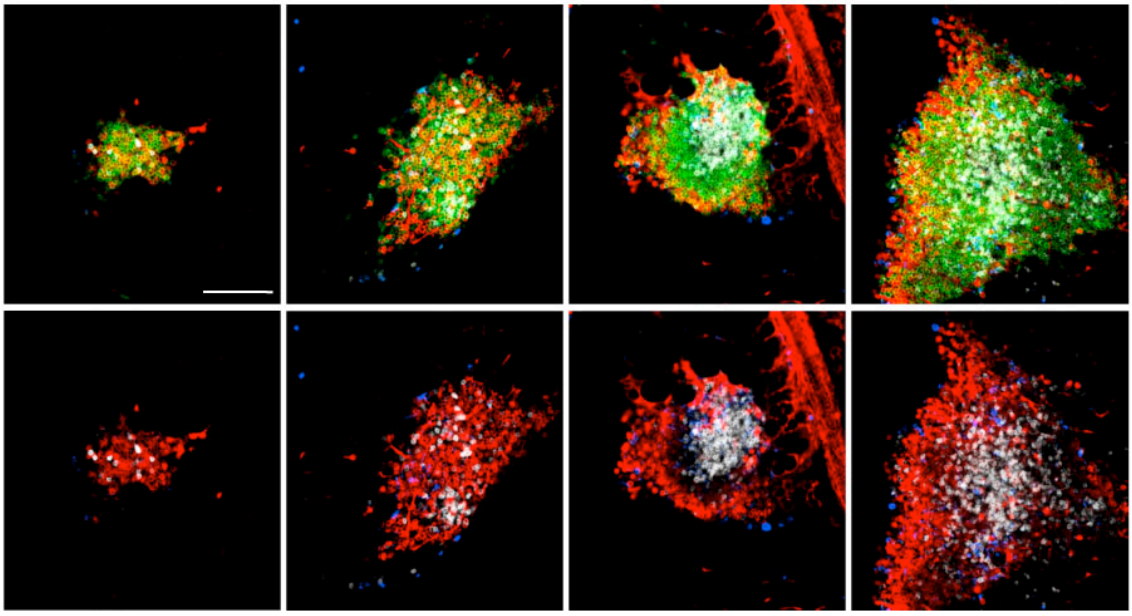

Supplementary Figure 1

FALC morphology

Whole mount immunofluorescence staining showing a representative array of FALCs harvested from the mesenteries of a single C57BL/6J (WT) mouse with $CD11b^+$ myeloid cells (blue), $CD45^+$ hematopoietic cells (green), IgM^+ B cells (red), and $CD4^+$ T cells (white) on the top row and without CD45 staining on the bottom row. Pictures are representative of 6 mice. Scale bar 50 μm.

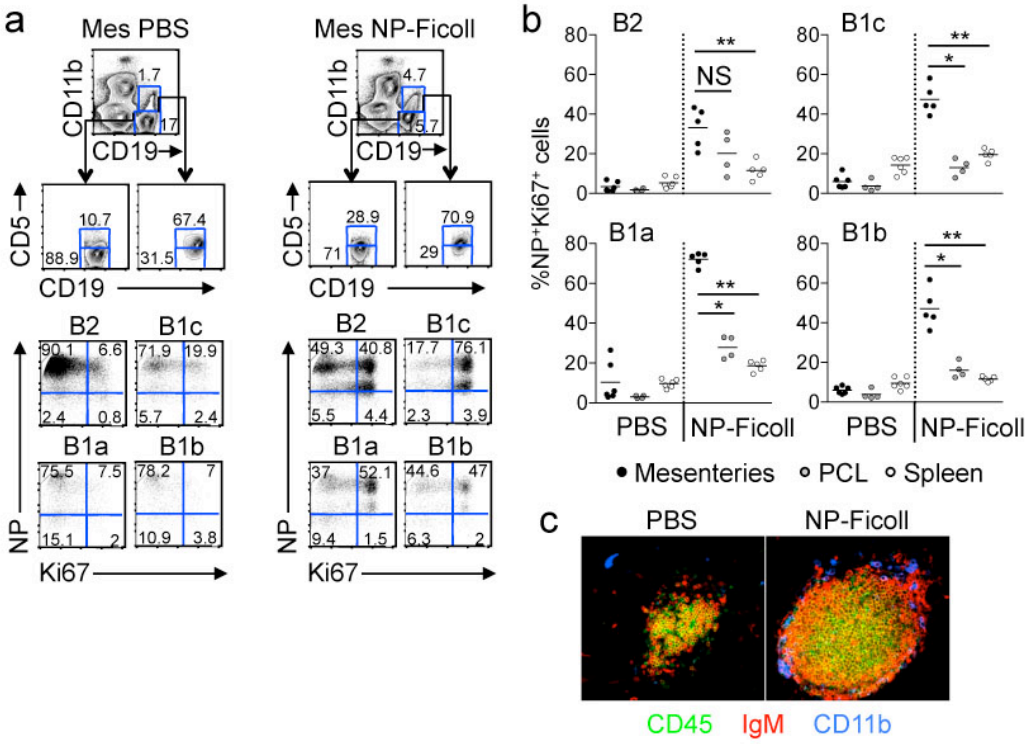

Supplementary Figure 2

B cell activation in FALCs upon peritoneal immune challenge

(**a**) Flow cytometry of the mesenteries of QM/QM ($IgH^{NP/NP}$ $Ig\kappa^{-/-}$) mice 24 hours post PBS (left panel) and NP-Ficoll (right panel) IP injection. In the $CD45^+$ hematopoietic fraction, the different B cell subsets were identified according to the expression of CD19 and CD11b (first row), CD19 and CD5 (second row). The percentages of NP^+Ki67^+ cells in the B2 ($CD19^+CD11b^-CD5^-$), B1c ($CD19^+CD11b^-CD5^+$), B1a ($CD19^+CD11b^+CD5^+$) and B1b ($CD19^+CD11b^+CD5^-$) cell subsets are shown (third and forth row). Image representative of 2 independent experiments (n=6, 5). (**b**) Quantification of the percentage of NP^+Ki67^+ activated B cells in the mesenteries, peritoneal cavity lavage (PCL) and spleen of QM/QM mice 24 hours after PBS or NP-Ficoll injections. Data are representative of 2 independent experiments (n=6, 5). Each symbol represents an individual mouse. Mann-Whitney nonparametric two-tailed test, B2 p=0.1905 and p=0.0079, B1c p=0.0159, p=0.0079, B1a p=0.0159, p=0.0079, B1b p=0.0159, p=0.0079. (**c**) Whole mount immunofluorescence staining showing FALCs from QM/QM mice after PBS or NP-Ficoll injection with $CD11b^+$ myeloid cells (blue), $CD45^+$ hematopoietic cells (green) and IgM^+ B cells (red). Pictures representative of 8 clusters from 4 mice for each condition. Scale bar 50 µm. *p < 0.05, **p < 0.01, ***p< 0.001, ****p < 0.0001, and NS not significant.

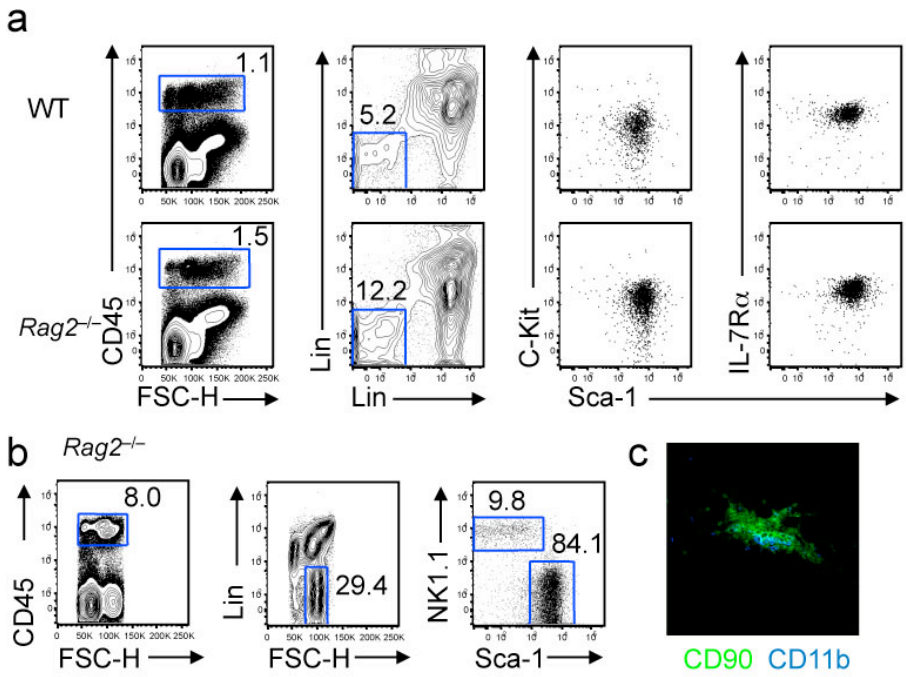

Supplementary Figure 3

ILC2 in VAT and FALCs

(**a**) Flow cytometry of the mesenteries showing CD45$^+$Lin$^-$c-Kit$^+$Sca-1$^+$IL-7Rα^+ ILC2 in WT (first row) and *Rag2*$^{-/-}$ (second row) mice (NK1.1 and CD4 present in Lin cocktail). Data representative of 4 mice (**b**) Flow cytometric analysis of the mesenteries showing CD45$^+$Lin$^-$Sca-1$^+$NK1.1$^-$ ILC2 and CD45$^+$Lin$^-$Sca-1-$^+$NK1.1$^+$ NK cells in *Rag2*$^{-/-}$ mice. Data representative of 4 mice (**c**) Whole mount immunofluorescence staining showing FALCs in *Rag2*$^{-/-}$ with CD11b$^+$ myeloid cells (blue) and CD90$^+$ ILC (green). The picture is representative of 8 clusters from 4 mice. Scale bar 50 µm.

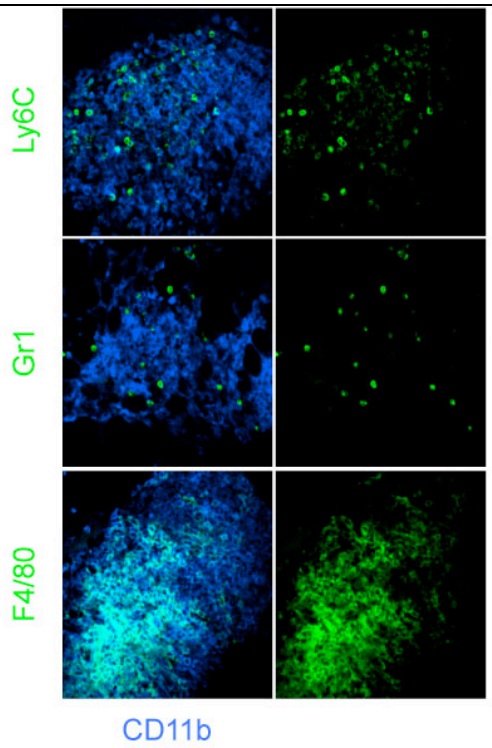

Supplementary Figure 4

Myeloid cells are recruited to FALCs upon inflammation

Whole mount immunofluorescence staining showing FALCs containing CD11b^{+} myeloid cells (blue) and Ly6C^{+} monocytes (first row, green), Gr1^{+} granulocytes (second row, green) or F4/80^{+} macrophages (third row, green) after zymosan injection. Pictures are representative of 8 clusters from 4 mice. Scale bar 50 µm.

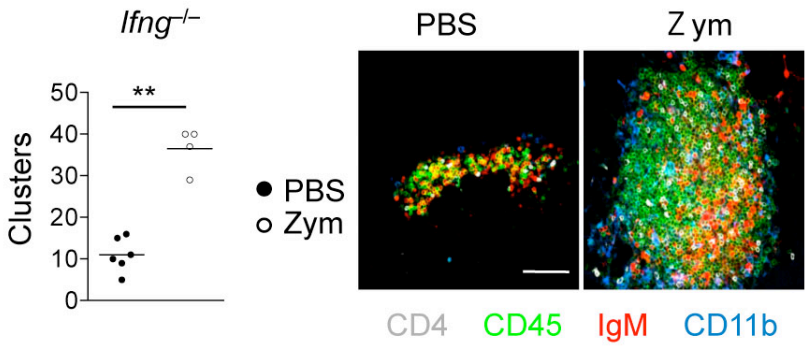

Supplementary Figure 5

IFN-γ is not necessary for FALC formation upon inflammation

Number of clusters found in the mesenteries of *Ifng*$^{-/-}$ mice and whole mount immunofluorescence staining showing FALCs with CD11b^{+} myeloid cells (blue), CD45^{+} hematopoietic cells (green), IgM^{+} B cells (red), and CD4^{+} T cells (white) 72 hours after IP injection of PBS or zymosan. Data corrrespond to control (n=6) and treated (n=4) mice pooled from 2 independent experiments. Each symbol represents an individual mouse Mann-Whitney nonparametric two-tailed test, p=0.0095. Pictures are representative of 8 clusters from 4 mice. Scale bar 50 µm. Scale bar 50 µm. $^{**}p < 0.01$.

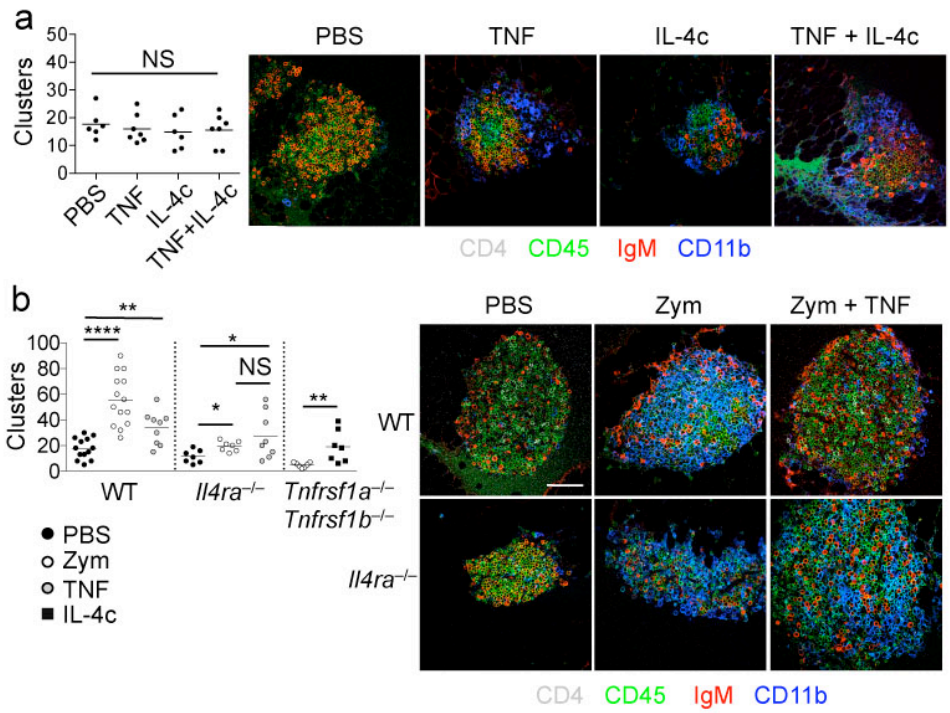

Supplementary Figure 6

Partial rescue of inflamation-induced FALC formation with IL-4c in the absence of TNF signaling

(**a**) Number of clusters found in the mesenteries of C57BL/6J (WT) mice and whole mount immunofluorescence staining showing FALCs with CD11b^{+} myeloid cells (blue), CD45^{+} hematopoietic cells (green), IgM^{+} B cells (red), and CD4^{+} T cells (white) four days after PBS, TNF, IL-4c and both TNF and IL4c injections. Data correspond to control (n=6) and TNF (n=6), IL-4c (n=7) and TNF+IL-4c (n=7) treated mice, pooled from 2 independent experiments. Mann-Whitney nonparametric two-tailed test, PBS and TNF p=0.4248, PBS and IL-4c p=0.4156, PBS and TNF+IL-4c p= 0.7964. Pictures are representative of 8 clusters from 4 mice for each condition. (**b**) Number of clusters found in the mesenteries of C57BL/6J (WT), *Il4ra*$^{-/-}$ and *Tnfrsf1a*$^{-/-}$ *Tnfrsf1b*$^{-/-}$ mice and whole mount immunofluorescence staining as in **a**, 4 days after PBS, zymosan, zymosan+TNF, and zymosan+IL-4c injections. Data correspond to PBS (n=13), zymosan (n=15) and zymosan+TNF (n=9) treated WT mice pooled from 3 independent experiments, and to PBS (n=7), zymosan (n=7) and zymosan+TNF (n=8) treated *Il4ra*$^{-/-}$ mice pooled from 2 independent experiments, and to zymosan (n=7) and zymosan+IL-4c (n=7) treated *Tnfrsf1a*$^{-/-}$ *Tnfrsf1b*$^{-/-}$ mice pooled from 2 independent experiments. Each symbol represents an individual mouse. Mann-Whitney nonparametric two-tailed test WT PBS and zymosan p<0.0001, WT PBS and zymosan+TNF p=0.0052, *Il4ra*$^{-/-}$ PBS and zymosan p=0.0105, *Il4ra*$^{-/-}$ PBS and zymosan+TNF p=0.0365, *Il4ra*$^{-/-}$ zymosan and zymosan+TNF p=0.7574, and *Tnfrsf1a*$^{-/-}$ *Tnfrsf1b*$^{-/-}$ zymosan and zymosan+IL-4c p=0.0029. Pictures are representative of 8 clusters from 4 mice for each condition. Scale bar 50 µm. **p* < 0.05, ***p* < 0.01, ****p*< 0.001 and *****p* <0.0001, NS not significant.

Supp. Table 1. Antibody List

Reagent	Clone	Conjugate	Source
CD1d-PBS57 tetramer		APC	NIH Tetramer Facility, Atlanta, GA, USA
Donkey anti-Goat		AlexaFluor555	Invitrogen
Donkey anti-IgM	Polyclonal	Rhodamine Red	Jackson Laboratories
Goat anti-Cxcl13	Polyclonal	Unconjugated	R&D Systems
Mouse anti-Ki67	B56	Alexa647	BD Pharmingen
Mouse anti-NK1.1	PK136	PE	eBiosciences
NP		PE	Biosearch Technologies
Rat anti-CD11b	M1/70	eFluor450	eBiosciences
		PerCP-Cyanine5.5	eBiosciences
Rat anti-CD138	281-2	PE	eBiosciences
Rat anti-CD19	eBio1D3	PECy7	eBiosciences
Rat anti-CD31	390	Biotin	eBiosciences
Rat anti-CD38	90	PerCP-eFluor 710	eBiosciences
Rat anti-CD4	GK1.5	eFluor660	eBiosciences
Rat anti-CD45	RA3-6B2	eFluor450	eBiosciences
	30-F11	PerCP	BD Pharmingen
Rat anti-CD45.2	104	FITC	eBiosciences
	104	Brilliant Violet 650	Biolegend
Rat anti-CD5	53-7.3	Biotin	eBiosciences
Rat anti-CD90.2	30-H12	FITC	eBiosciences
Rat anti-CD117 (c-Kit)	ACK2	APC	eBiosciences
Rat anti-CD127 (IL-7Ra)	A7R34	PE-Cyanine7	eBiosciences
Rat anti-F4/80	BM8	FITC	eBiosciences
		PE-Cyanine7	
Rat anti-GL7	GL-7	eFluor450	
Rat anti-Ly-6C	HK1.4	Alexa Fluor488	eBiosciences
		Alexa Fluor647	
Rat anti-Ly-6G (Gr-1)	RB6-8C5	FITC	eBiosciences
Rat anti-Ly6G	1A8	APC/Cy7	Biolegend
Rat anti-Lyve-1	ALY7	eFluor660	eBiosciences
Rat anti-Sca-1	D7	FITC	eBiosciences
Rat anti-Siglec-F	ES22-10D8	PE	Miltenyi

Streptavidin	AlexaFluor555	Invitrogen
Streptavidin	APC.Cy7	eBiosciences
Streptavidin	Pacific Orange	Invitrogen

Reagent	Clone	Conjugate	Source
Lineage 1			
Armenian Hamster anti-CD3e	145-2C11	PE	eBiosciences
Armenian Hamster anti-CD11c	N418	PE	eBiosciences
Rat anti-CD19	eBio1D3	PE	eBiosciences
Rat anti-Ly-6G (Gr-1)	RB6-8C5	PE	eBiosciences
Rat anti-NK1.1	PK136	PE	eBiosciences
Rat anti-TER-119	TER-119	PE	eBiosciences
Lineage 2			
Armenian Hamster anti-TCRb	H57-597	Biotin	eBiosciences
Armenian Hamster anti-TCRgd	UC7-13D5	Biotin	eBiosciences
Rat anti-B220	RA3-6B2	Biotin	eBiosciences
Rat anti-CD5	53-7.3	Biotin	eBiosciences
Rat anti-CD8a	53-6.7	Biotin	eBiosciences
Rat anti-CD11b	M1/70	Biotin	eBiosciences

Mouse IgG-AP	Southern Biotech
Goat anti-mouse IgM-AP	Southern Biotech
PE	Prozyme